JAMES | Journal of Advances in Modeling Earth Systems

RESEARCH ARTICLE
10.1029/2022MS003150

Special Section:
Understanding carbon-climate feedbacks

Do State-Of-The-Art Atmospheric CO_2 Inverse Models Capture Drought Impacts on the European Land Carbon Uptake?

Wei He[1,2,3], Fei Jiang[1,2,4], Weimin Ju[1,2], Brendan Byrne[5], Jingfeng Xiao[6], Ngoc Tu Nguyen[7], Mousong Wu[1,2], Songhan Wang[8], Jun Wang[1,2], Christian Rödenbeck[9], Xing Li[10], Marko Scholze[11], Guillaume Monteil[11], Hengmao Wang[1,2], Yanlian Zhou[2], Qiaoning He[12], and Jing M. Chen[13,14]

[1]International Institute for Earth System Science, Nanjing University, Nanjing, China, [2]Jiangsu Provincial Key Laboratory of Geographic Information Science and Technology, Key Laboratory for Land Satellite Remote Sensing Applications of Ministry of Natural Resources, School of Geography and Ocean Science, Nanjing University, Nanjing, China, [3]State Key Laboratory of Remote Sensing Science Jointly Sponsored by Beijing Normal University and Aerospace Information Research Institute, Chinese Academy of Sciences, Beijing, China, [4]Frontiers Science Center for Critical Earth Material Cycling, Nanjing University, Nanjing, China, [5]Jet Propulsion Laboratory, California Institute of Technology, Pasadena, CA, USA, [6]Earth Systems Research Center, Institute for the Study of Earth, Oceans, and Space, University of New Hampshire, Durham, NH, USA, [7]State Key Laboratory of Hydrology-Water Resources and Hydraulic Engineering, College of Hydrology and Water Resources, Hohai University, Nanjing, China, [8]Jiangsu Collaborative Innovation Center for Modern Crop Production, Key Laboratory of Crop Physiology and Ecology in Southern China, Nanjing Agricultural University, Nanjing, China, [9]Max Planck Institute for Biogeochemistry, Jena, Germany, [10]Research Institute of Agriculture and Life Sciences, Seoul National University, Seoul, South Korea, [11]Department of Physical Geography and Ecosystem Science, Lund University, Lund, Sweden, [12]School of Urban and Environmental Sciences, Huaiyin Normal University, Huaian, China, [13]Department of Geography and Planning, University of Toronto, Toronto, ON, Canada, [14]School of Geographical Sciences, Fujian Normal University, Fuzhou, China

Key Points:

- Global inversions with only limited surface CO_2 observations give divergent estimates of drought impacts on the European carbon uptake
- Regional inversions assimilating denser CO_2 observations over Europe demonstrate some improved consistency but are still deficient
- The inversions assimilating satellite XCO_2 or environmental variables in addition to surface CO_2 largely improve the estimates

Supporting Information:

Supporting Information may be found in the online version of this article.

Correspondence to:

F. Jiang,
jiangf@nju.edu.cn

Citation:

He, W., Jiang, F., Ju, W., Byrne, B., Xiao, J., Nguyen, N. T., et al. (2023). Do state-of-the-art atmospheric CO_2 inverse models capture drought impacts on the European land carbon uptake? *Journal of Advances in Modeling Earth Systems*, *15*, e2022MS003150. https://doi.org/10.1029/2022MS003150

Received 21 APR 2022
Accepted 19 MAY 2023

Author Contributions:

Conceptualization: Wei He, Fei Jiang

Abstract

The European land carbon uptake has been heavily impacted by several recent severe droughts, yet quantitative estimates of carbon uptake anomalies are uncertain. Atmospheric CO_2 inverse models (AIMs) provide observation-based estimates of the large-scale carbon flux dynamics, but how well they capture drought impacts on the terrestrial carbon uptake is poorly known. Here we assessed the capacity of state-of-the-art AIMs in monitoring drought impacts on the European carbon uptake over 2001–2015 using observations of environmental variability and vegetation function and made comparisons with bottom-up estimates of carbon uptake anomalies. We found that global inversions with only limited surface CO_2 observations give divergent estimates of drought impacts. Regional inversions assimilating denser CO_2 observations over Europe demonstrated some improved consistency, with all inversions capturing a reduction in carbon uptake during the 2012 drought. However, they failed to capture the reduction caused by the 2015 drought. Finally, we found that a set of inversions that assimilated satellite XCO_2 or assimilated environmental variables plus surface CO_2 observations better captured carbon uptake anomalies induced by both the 2012 and 2015 droughts. In addition, the recent Orbiting Carbon Observatory—2 XCO_2 inversions showed good potential in capturing drought impacts, with better performances for larger-scale droughts like the 2018 drought. These results suggest that surface CO_2 observations may still be too sparse to fully capture the impact of drought on the carbon cycle at subcontinental scales over Europe, and satellite XCO_2 and ancillary environmental data can be used to improve observational constraints in atmospheric inversion systems.

Plain Language Summary

Atmospheric CO_2 inverse models (AIMs) are useful tools for quantifying the response of large-scale carbon uptake to climate extremes, but their capacity for monitoring drought impacts, particularly at regional scales, is not fully explored. In this study, we assessed the capacity of state-of-the-art AIMs for monitoring drought impacts on the European land carbon uptake over 2001–2015 using a large array of observational and model data sets. We found: (a) global inversions with only limited surface CO_2 observations face a great challenge in monitoring drought impacts on the European carbon uptake; (b) Regional inversions assimilated denser CO_2 observations over Europe, for the EUROCOM project, demonstrated some improved consistency but are still deficient, showing divergent estimates in interannual variability of carbon uptake for most years; and (c) A set of inversion systems that assimilated satellite XCO_2 or assimilated environmental variables plus surface CO_2 observations better captured annual and seasonal

Data curation: Fei Jiang, Brendan Byrne, Jingfeng Xiao, Mousong Wu, Christian Rödenbeck, Xing Li, Marko Scholze, Guillaume Monteil
Formal analysis: Wei He
Funding acquisition: Wei He, Fei Jiang, Weimin Ju
Methodology: Wei He, Brendan Byrne
Project Administration: Fei Jiang, Weimin Ju
Resources: Fei Jiang, Weimin Ju, Ngoc Tu Nguyen
Writing – original draft: Wei He
Writing – review & editing: Fei Jiang, Weimin Ju, Brendan Byrne, Jingfeng Xiao, Ngoc Tu Nguyen, Mousong Wu, Songhan Wang, Jun Wang, Christian Rödenbeck, Xing Li, Marko Scholze, Guillaume Monteil, Hengmao Wang, Yanlian Zhou, Qiaoning He, Jing M. Chen

anomalies caused by droughts. Our study demonstrates that surface CO_2 observations may still be too sparse to fully capture the impact of drought on the carbon cycle at subcontinental scales over Europe, whereby satellite XCO_2 and ancillary environmental data can offer observational constraints for improving the estimates.

1. Introduction

In recent decades, large-scale extreme droughts have frequently hit various regions over the globe, and Europe is becoming a hotspot (Ciais et al., 2005; Flach et al., 2018; Laaha et al., 2017; Peters et al., 2020; S. Wang et al., 2020). Such droughts have been known to strongly influence the inter-annual variations (IAV) of terrestrial carbon uptake at both regional (Wolf et al., 2016) and global (Ahlström et al., 2015) scales. Accurately monitoring the behavior of terrestrial ecosystems in response to droughts is critical for understanding the carbon-climate interaction and feedbacks (Xiao et al., 2016).

Atmospheric CO_2 inverse models (AIMs) infer the surface carbon dioxide (CO_2) fluxes from atmospheric mole fraction observations through adjusting prior surface fluxes (often provided by terrestrial biosphere models [TBMs]) to minimize the gap between simulated concentration and observed concentration within model–data fusion frameworks. These models have been utilized for more than two decades in carbon cycle research (Chevallier et al., 2019; Gurney et al., 2004; Peters et al., 2007; Rödenbeck et al., 2003; van der Laan-Luijkx et al., 2017). Over most of their history, AIMs have primarily been employed to study the continental-to-global scale carbon cycle by assimilating CO_2 measurements from a sparse network of surface sites. However, AIMs are increasingly being applied to regional carbon flux estimation (Byrne, Liu, Lee, et al., 2020; Friedlingstein et al., 2019; He, Jiang, Wu, et al., 2022; He, van der Velde, et al., 2018; Monteil et al., 2020) and assess carbon cycle response to climate extremes (He, Ju, et al., 2018; J. Liu et al., 2018; Molina et al., 2015; van der Laan-Luijkx et al., 2015; Wolf et al., 2016).

AIMs offer a formal way to assess the impact of climate extremes (e.g., drought) on the carbon cycle. However, the sparse sampling of CO_2 measurements has generally been insufficient to capture the carbon cycle response to these regional climate extremes. Recently, increasing observational coverage from an expanded network of surface sites has been improving our ability to capture regional fluxes (Monteil et al., 2020). Further, assimilating satellite measurements of column-averaged dry-air mole fractions of CO_2 (XCO_2) (Byrne, Liu, Lee, et al., 2020; Jiang et al., 2021; J. Liu et al., 2018) or land surface data (Rödenbeck et al., 2018b; Scholze et al., 2019) are also now being utilized to refine CO_2 flux estimates. Still, the capacity of current AIMs in capturing the impacts of large-scale droughts on ecosystems has not been fully studied.

Assessing the accuracy of carbon flux products is critical for improving our understanding of the link between the terrestrial carbon cycle and climate change. Validation of large-scale carbon fluxes is a common challenge. As suggested by Schewe et al. (2019), research efforts of model development and evaluation need to be shifted away from mean conditions toward extremes. For example, several studies have systematically examined state-of-the-art land surface models for monitoring the carbon cycle responses to typical large-scale drought events (He et al., 2021; Peters et al., 2020; Schewe et al., 2019). Similarly, previous studies have shown that the performance of AIMs can be evaluated through comparisons of IAV in the driving environmental variables and against independent CO_2 flux estimates. For example, Byrne et al. (2019) evaluated the ability of AIMs to reproduce CO_2 flux IAV against variability in the environmental drivers (e.g., temperature and moisture) as well as observations of vegetation function (e.g., solar-induced chlorophyll fluorescence [SIF]) and independent CO_2 flux estimates (e.g., FLUXCOM). They found that comparisons against these data sets proved to be an effective method for evaluating the performance of AIMs, and were even able to characterize the impact of the flux inversion set-up on IAV estimates. Similarly, Yin et al. (2020) demonstrated that anomalies in SIF were closely linked to net ecosystem production (NEP) anomalies caused by extreme flooding in the Midwest USA during the spring of 2019. These studies demonstrate that we should expect a substantial level of agreement among variations in environmental quantities, measurements of vegetation function, and IAV estimated by AIMs.

Recent droughts in Europe provide us with a good opportunity for evaluating the state-of-the-art capacities of AIMs in capturing drought-induced IAV and seasonal variations of land-atmosphere carbon fluxes. Newly developed remote sensing products provide useful information on the spatial and temporal variations of carbon fluxes, which can be used to benchmark carbon flux products. An increasing array of satellite land surface metrics, such as SIF, near-infrared reflectance index (NIRv), microwave satellite soil moisture (SM), and total

terrestrial water storage (TWS), are available for assessing the impacts of climate extremes on terrestrial ecosystems (Palmer, 2018; Peters et al., 2020; Smith et al., 2020; S. Wang et al., 2020). Moreover, satellite data-driven GPP products, including FluxSat (Joiner et al., 2018) and GOSIF GPP (Li & Xiao, 2019b), can be used to evaluate the performance of AIMs-estimated NEP in response to droughts. That is because, there is a strong link between the temporal variations of NEP and GPP from both models (Piao et al., 2020; Wieder et al., 2021; L. Zhang et al., 2019) and observations (Baldocchi, 2008; Baldocchi et al., 2018; Shiga et al., 2018). In addition, in situ eddy covariance flux data can be used to indicate drought-induced changes in the seasonal cycles of carbon fluxes. A study synthesizing different sources of observations and diverse models under a unified drought context would help advance our understanding of the responses of the terrestrial carbon cycle to droughts and the performance of carbon cycle models.

In this study, we aimed to assess the capacities of state-of-the-art AIMs with diverse model formations and different assimilated data sources, including both in situ based and satellite-based, in capturing realistic terrestrial carbon uptake anomalies associated with European droughts during the period 2001–2015. To this end, observations of environmental variability and vegetation function and in situ eddy covariance flux data were used to evaluate the IAV and seasonal variation of NEP at regional scales, with bottom-up estimates of carbon uptake anomalies by the TRENDY models and the FLUXCOM data set for comparisons.

2. Data and Methods

2.1. Study Area

Our study area spans over 33°–73°N, 15°W–35°E (Figure S1 in Supporting Information S1), which covers most areas of Europe. Since 2003, several severe drought events occurred in this area, which caused a large loss of terrestrial carbon uptake (Bastos et al., 2020; Ciais et al., 2005). In order to evaluate the model performance on capturing drought impacts over different parts of Europe, the study area is divided into four subregions (Figure S1b in Supporting Information S1) following EUROCOM: northern Europe (Scandinavia, Finland, and the Baltic states), southern Europe (the Iberian Peninsula, Italy, Greece, Romania, and the Balkan states), western Europe (France, Benelux, the UK, and Ireland), and central Europe (the remaining countries, up to the eastern border of Poland) (Monteil et al., 2020).

2.2. Carbon Fluxes Constrained by Atmospheric CO_2 Observations

We included estimated carbon fluxes from inversions constrained by either in situ CO_2 or satellite data. The data sets used in this study are summarized in Table 1, with additional details on the inversion systems summarized in Table S1 in Supporting Information S1 (global in situ based inversions), Table S2 in Supporting Information S1 (regional in situ based inversions), and Table S3 in Supporting Information S1 (satellite-based inversions).

Carbon flux estimates from five in situ CO_2 based global inversions were examined in this study, including CarbonTracker Europe (CTE2018) (Peters et al., 2010; van der Laan-Luijkx et al., 2017), CarbonTracker (CT2019B) (Peters et al., 2007), CAMS (Chevallier et al., 2010), and Jena CarboScope standard inversion (Rödenbeck et al., 2003). The newly extended inversions of NEE–T (Rödenbeck et al., 2018b) and NEE–T–W (Rödenbeck et al., 2020) of Jena CarboScope were used for comparison. The CarbonTracker Europe (CTE) (Peters et al., 2010; van der Laan-Luijkx et al., 2017) developed at Wageningen University (http://www.carbontracker.eu) assimilates global air samples of CO_2 mole fractions to adjust prior surface carbon fluxes. Here we used the monthly CTE2018 fluxes with a spatial resolution of 1° × 1°. Another similar atmospheric CO_2 inversion product, CarbonTracker (CT) 2019 (Jacobson et al., 2020; Peters et al., 2005, 2007), is developed at NOAA (www.carbontracker.noaa.gov). We used the monthly CT2019B fluxes at a spatial resolution of 1° × 1° in this study. Four other inversion-based flux estimates, from CAMS (v18r2) and Jena CarboScope (s99_v4.3, NEE–T_v4.3, and NEE–T–W_v4.3), were also used. The CAMS (v18r2) product provides global monthly fluxes at a spatial resolution of 3.75° × 1.875°. The Jena CarboScope product provides global monthly fluxes at a spatial resolution of 5° × 4°. The Jena s99_v4.3 inversion starts in 1999 and uses observations from 50 stations that cover this entire period. The Jena NEE–T inversion differs from the standard one only by replacing the explicitly time-dependent inter-annual NEE variations with a linear NEE–T (surface temperature) regression term plus residual terms, and by using a larger set of measurement stations (Rödenbeck et al., 2018b). The surface temperature data is from Goddard Institute for Space Studies analysis (Hansen et al., 2010; Lenssen et al., 2019). In addition to the temperature constraint,

Journal of Advances in Modeling Earth Systems
10.1029/2022MS003150

Table 1
Specifics of the Carbon Fluxes, Satellite Land Surface Data, Meteorological Data, and In Situ Flux Data Used in This Study

	Data set	Spatial resolution	Temporal resolution	Time span	References
Global inversions	CTE2018	1° × 1°	Monthly	2000–2017	van der Laan-Luijkx et al. (2017)
	CT2019B	1° × 1°	Monthly	2000–2018	Peters et al. (2007) and Jacobson et al. (2020)
	CAMS_v18r2	3.75° × 1.875°	Monthly	2000–2018	Chevallier et al. (2010)
	Jena CarboScope Standard v4.3 (s99)	5° × 4°	Monthly	1957–2018	Rödenbeck et al. (2003)
	Jena CarboScope NEE–T v4.3	5° × 4°	Monthly	1957–2018	Rödenbeck et al. (2018b)
	Jena CarboScope NEE–T–W v4.3	5° × 4°	Monthly	1957–2018	Rödenbeck et al. (2020)
Regional inversions	EUROCOM inversions	0.5° × 0.5°	Monthly	2006–2015	Monteil et al. (2020)
Satellite inversions	GCASv2	1° × 1°	Monthly	2010–2015	Jiang et al. (2021)
	Byrne2020	5° × 4°	Monthly	2010–2015	Byrne, Liu, Lee, et al. (2020)
	CMS-Flux NBE 2020	5° × 4°	Monthly	2010–2015	J. Liu et al. (2020)
	CCDAS_SM + VOD	0.25° × 0.25°	Monthly	2010–2015	Scholze et al. (2019)
Bottom-up NEP estimates	TRENDY v6	0.5° × 0.5°	Monthly	1901–2016	Sitch et al. (2015)
	FLUXCOM2020	0.5° × 0.5°	Monthly	2001–2018	Jung et al. (2020)
Satellite GPP data sets	FluxSat	0.5° × 0.5°	8-day	2001–2020	Joiner et al. (2018)
	GOSIF GPP v2	0.5° × 0.5°	Monthly	2001–2018	Li and Xiao (2019b)
Environmental variables	CRUNCEP v9	0.5° × 0.5°	Monthly	1901–2017	Wei et al. (2014)
	GLEAM v3.3a root-zone SM	0.25° × 0.25°	Daily	1981–2018	Martens et al. (2017)
Vegetation variables	MOD13C2 v6	0.05° × 0.05°	Monthly	2001–2020	Huete et al. (2002)
	CSIF v2	0.05° × 0.05°	4-day	2001–2020	Y. Zhang et al. (2018)
In situ flux measurements	Drought2018-FLUXNET-ICOS	None	Monthly	Diverse, including 2001–2015	Heiskanen et al. (2021)

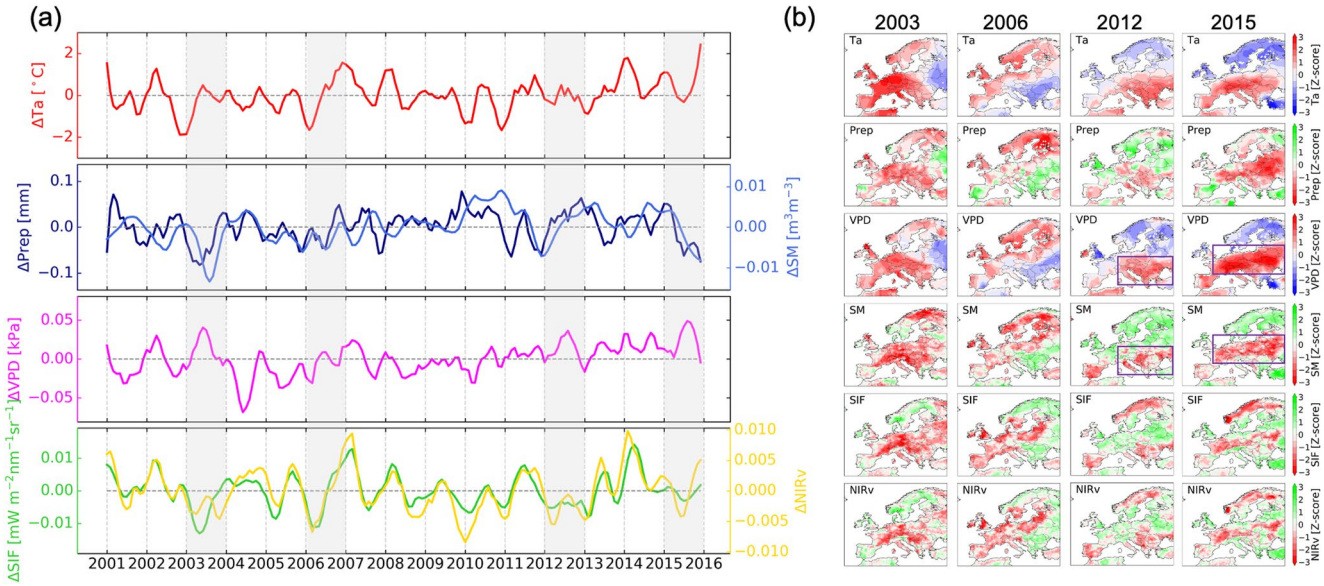

Figure 1. Spatiotemporal anomalies of air temperature (Ta), precipitation (Prep), soil moisture (SM), vapor pressure deficit (VPD), reconstructed contiguous solar-induced fluorescence, and near-infrared reflectance index (NIRv) in Europe over 2001–2015. Monthly anomalies are calculated as the variable value subtract multiple-year mean over the whole period. The spatial patterns show for the summer time (June–August). The boxes indicate the selected drought-impacted regions in 2012 and 2015 used for further analyses. The regions were selected according to the anomalies in VPD and SM.

the Jena NEE–T–W inversion uses the six-monthly accumulated Standardized Precipitation-Evapotranspiration Index (SPEI) as an extra constraint (Rödenbeck et al., 2020). Here, the Jena NEE–T/NEE–T –W inversions were used as references due to their known improved performances in characterizing the IAV of large-scale NEP compared to the standard inversion (Rödenbeck et al., 2018b, 2020).

We included seven in situ CO_2 based regional inversions from the EUROCOM project (https://eurocom.icos-cp.eu/; Monteil et al., 2020), including CarboScope-Regional (Kountouris et al., 2018), LUMIA (Monteil & Scholze, 2021), EnKF-RAMS (Meesters et al., 2012), FLEXINVERT (Thompson & Stohl, 2014), PYVAR-CHIMERE (Fortems-Cheiney et al., 2021), and CTE for EUROCOM (Smith et al., 2020). These inversions used enhanced surface CO_2 observations of 39 stations over Europe (see Figure 1b), and their inversion systems built upon either Eulerian or Lagrangian models.

We used three satellite XCO_2 based inversions, including the one from combined GOSAT, surface, and TCCON data with three different prior biosphere fluxes generated by Byrne, Liu, Lee, et al. (2020) (hereafter Byrne2020), GCASv2 (Jiang et al., 2021; Jiang, Ju, et al., 2022), and CMS-Flux NBE 2020 (J. Liu et al., 2020). The Byrne2020 flux was estimated at 4° × 5° at a 14-day scale from 2010 to 2015 based on the GEOS-Chem atmospheric transport model and Bayesian data assimilation technique. GCASv2 assimilates GOSAT XCO_2 retrievals, while CMS-Flux assimilates the XCO_2 retrievals from both GOSAT and OCO-2. More details about the system setup for these satellite inversions can be found in Table S3 in Supporting Information S1. We aggregated the fluxes temporally to monthly fluxes. For Byrne2020, the arithmetic average of the three inversions with different prior biosphere fluxes was used for the analyses.

In addition, we employed the estimated carbon fluxes constrained by in situ CO_2 and satellite SM and vegetation data within the Carbon Cycle Data Assimilation System (CCDAS) (Rayner et al., 2005). CCDAS is a variational data assimilation system built on the terrestrial biosphere model, Biosphere Energy Transfer and Hydrology scheme (Knorr, 2000), and coupled to the atmospheric transport model, Transport Model, version 3 (Heimann & Korner, 2003) for assimilating atmospheric CO_2 data. CCDAS jointly assimilated remotely sensed SM and vegetation optical depth (VOD) data, combined with in situ CO_2 air samples, to constrain global surface carbon fluxes through parameter optimization of its underlying biosphere model. The SM data is from the SMOS-IC product (Souza et al., 2018). The VOD data is from the SMOS-IC L-VOD product (Wigneron et al., 2021), for which the annual mean VOD was assimilated in CCDAS. This result proved to well constrain the European terrestrial carbon sink (Scholze et al., 2019). The readers are referred to Scholze et al. (2019) for more details.

In this study, we refer land carbon uptake to NEP. In order to make the targeted fluxes consistent with each other across all inversions, we summed up fire emission and biosphere fluxes (net biome production) for some inversion results, for example, for CTE2018, CT2019B, and the EUROCOM inversions.

2.3. Carbon Fluxes Simulated by Terrestrial Biosphere Models (TRENDY DGVMs)

We used terrestrial carbon fluxes simulated by seven process-based dynamic global vegetation models, including ORCHIDEE (Krinner et al., 2005), ORCHIDEE-MICT (Krinner et al., 2005), CABLE (Y. Wang et al., 2010), DLEM (Tian et al., 2015), ISAM (Jain et al., 2013), VEGAS (N. Zeng et al., 2005), and VISIT (Kato et al., 2013), which were involved in the TRENDY v6 project (Sitch et al., 2015). The simulations under scenario S3, which considered impacts from climate, CO_2, and land use change, were used. These simulations were conducted using the CRUNCEP v8 data set and provided monthly fluxes at a spatial resolution of $0.5° \times 0.5°$.

2.4. Machine Learning-Based Upscaling of Eddy-Covariance Measurements (FLUXCOM)

The FLUXCOM product (www.fluxcom.org) is produced by upscaling FLUXNET eddy-covariance flux measurements over the globe. Using machine learning (ML) algorithms, it scales in situ flux measurements into time-resolved $0.5° \times 0.5°$ grids of NEP, ecosystem respiration (Reco), and GPP with remote sensing data and meteorological data (FLUXCOM-RS + METEO) (Jung et al., 2019, 2020; Tramontana et al., 2016). Here we used the latest data version, FLUXCOM2020. There are 3 ML algorithms (Multivariate Adaptive Regression Splines [MARS], Artificial Neural Networks [ANN], and Random Forests [RF]) for generating the FLUXCOM-RS + METEO product, and two methods used for separating GPP and Reco from tower-based NEP (Lasslop et al., 2010; Reichstein et al., 2005). FLUXCOM-RS + METEO is generated using two reanalysis meteorological data, CRUJRA v1.1 and ERA5, respectively. In this study, we used the ensemble estimates generated with different ML algorithms and gross flux separating methods over the period from 2001 to 2015 at a monthly temporal resolution.

2.5. Satellite-Based GPP Models

Two satellite-based data-driven GPP models, FluxSat (Joiner et al., 2018) and GOSIF GPP (Li & Xiao, 2019b), were employed in this study. FluxSat is derived from a data-driven approach relying on FLUXNET measurements and Moderate Resolution Imaging Spectroradiometer (MODIS) reflectances in seven spectral bands and calibrated against FLUXNET measurements. It is noteworthy that FluxSat does not use any meteorological forcing. A dual-calibration procedure is applied by discriminating low versus high productive FLUXNET sites, where the identification is based on satellite SIF products derived from the Global Ozone Monitoring Experiment 2 observations. GOSIF GPP is derived from the global OCO-2 based SIF product (GOSIF) and the linear relationships between OCO-2 SIF and tower-based GPP. The GOSIF product (Li & Xiao, 2019a) is based on discrete OCO-2 SIF soundings, MODIS data, and meteorological reanalysis data. GOSIF GPP has a high spatial and temporal resolution (i.e., 0.05°, 8-day) over 2000–2020 (Li & Xiao, 2019b). We used the latest version (v2) for GOSIF GPP here.

2.6. Satellite Land Surface Data

Four satellite land surface metrics were employed for drought impact related analyses: microwave satellite SM, SIF, and NIRv.

The stress of soil water on carbon uptake was investigated using the Global Land-surface Evaporation Amsterdam Methodology (GLEAM) root-zone SM data in this study. GLEAM root-zone SM was produced from the satellite surface SM product ESA-CCI SM through data assimilation (Martens et al., 2017; Miralles et al., 2011). We used the v3.3a products with aggregated monthly fluxes at a spatial resolution of $0.25° \times 0.25°$ over 1981–2018 (Dorigo et al., 2017).

Remotely sensed SIF has shown great promise for probing spatiotemporal variations of GPP (Guanter et al., 2014; Li et al., 2018) and is also sensitive to water (Alden et al., 2016; J.-E. Lee et al., 2013; Sun et al., 2015) and temperature stresses (Song et al., 2018). Here we used a reconstructed contiguous SIF data set over 2000–2018

(Y. Zhang et al., 2018) based on OCO-2 data and MODIS data (named contiguous solar-induced fluorescence [CSIF], version 2), which covers the study period. We aggregated the data into monthly time steps.

Finally, we included a new photosynthesis indicator, near-infrared reflectance index (NIRv). NIRv is expressed as the product of NDVI and near infra-red reflectance (Badgley et al., 2017), which is proved to be a useful indicator of GPP and has been used to indicate global photosynthesis (Badgley et al., 2019; Y. Zeng et al., 2019). NIRv used here was calculated directly from the MODIS vegetation product (MOD13C2, v6).

2.7. Meteorological Data

We used air temperature and precipitation data with a spatial resolution of 0.5° × 0.5° from the CRUNECP reanalysis data set (v9) to assess the impacts of water and temperature anomalies on GPP. The CRUNCEP v9 data set was produced by the Institute Pierre Simon Laplace (IPSL) of France (Wei et al., 2014), which is a merged product of Climate Research Unit observation-based monthly 0.5° × 0.5° climate variables (New et al., 2000) (1901–2017) and the 6-hourly reanalysis of National Centers for Environmental Prediction. This data set was also used to drive the TRENDY models.

The vapor pressure deficit (VPD) was used to indicate atmospheric moisture limitations on vegetation growth and carbon uptake. It was derived from air temperature (Ta), specific humidity (Q), and atmospheric pressure (P) provided by the CRUNCEP data set. VPD is defined as the difference between the saturated vapor pressure (e_sat) and the actual atmospheric vapor pressure (e):

$$\mathrm{VPD} = \mathrm{e\_sat} - \mathrm{e} \tag{1}$$

First, the saturated vapor pressure (vpsat, in kPa) at a given temperature is calculated according to the Buck Equation (Buck, 1996):

$$\mathrm{e\_sat} = 0.61121^{*}\exp((18.678 - \mathrm{Ta}/234.5)^{*}(\mathrm{Ta}/(257.14 + \mathrm{Ta}))) \tag{2}$$

Then, the actual atmospheric vapor pressure (e, in kPa) is calculated using the equation derived from the relation between vapor pressure, specific humidity, and atmospheric pressure, described in Monteith and Unsworth (2008):

$$\mathrm{e} = \mathrm{Q}^{*}\mathrm{P}/[\varepsilon + (1-\varepsilon)^{*}\mathrm{Q}] \tag{3}$$

where ε is the ratio between the molecular weight of water vapor and that of dry air (0.622).

2.8. In Situ Flux Measurements

We included in situ eddy covariance flux measurements from the ICOS-Drought2018 project (https://www.icos-cp.eu/data-products/YVR0-4898) (Drought, 2020). A total of 19 stations with long-term observations generally spanned over the study period (at least having 5-year data) and data roughly covered the drought occurrence areas in 2012 and 2015 were chosen. These data cover different ecosystem types: 6 crop sites (BE-Lon, CH-Oe2, DE-Geb, DE-Kli, DE-RuS, and IT-BCi), 4 grass sites (CH-Fru, DE-Gri, DE-RuR, and IT-Tor), 3 deciduous broadleaf forest sites (DBF, including CZ-Stn, DE-Hai, and DE-Hzd), 6 evergreen needle leaf forest sites (ENF, including CZ-Bk1, DE-THa, DE-Obe, DE-RuW, NL-Loo, and RU-Fyo). Most of these sites locate in Central Europe. The locations of these sites are shown in Figure S1a in Supporting Information S1, and more details about these stations are provided in Table S4 in Supporting Information S1. Monthly NEE data from NEE_VUT_REF and monthly GPP data from GPP_NT_VUT_REF were used in this study. They were used as a reference to evaluate the seasonal variation of drought impacts on ecosystem carbon fluxes by grouping into forest and non-forest (crop/grass) categories.

2.9. Data Processing and Analysis Framework

To facilitate calculations, all data sets used in this study were resampled to 0.5° × 0.5° grids at a monthly step. The spatial aggregation was done by simply replicating and averaging over grid domains. For example, the process to resample a data set with a spatial resolution of 3.75° × 1.875° – 0.5° × 0.5° is: (a) splitting each grid into subgrids with 0.125° × 0.125°, which produces 20 × 15 subgrids and (b) averaging the values within each 4 × 4 square of the subgrids, which makes a 0.5° × 0.5° grid.

In this study, we focus on anomaly analyses related to the terrestrial carbon cycle and climate conditions. We calculated the anomalies of carbon fluxes, meteorological data, hydrological data, and vegetation metrics relative to the baseline, here using the mean values over the study period (2001–2015). For monthly anomalies, mean seasonal cycles were previously subtracted. The annual values were calculated by summing monthly anomalies. To calculate IAV and correlation between two time series variables that exclude the influence of external forcing (i.e., global warming), the anomalies of carbon fluxes and vegetation variables were linearly detrended using the "detrend" function within the "signal" collection of the "scipy" package in Python. To clearly present spatial differences of these anomalies among different variables, we also used the standardized anomalies (called "*Z*-score"), the anomalies divided by the standard deviation of the variable over the study period. In addition, Pearson's correlation coefficients were used to quantify the correlation relationship or temporal consistency between different data sets.

In the following, we first assess the drought conditions in Europe during 2001–2015 using environmental variables (e.g., temperature and water status) and vegetation function proxies (e.g., SIF and GPP). Then we take these environmental variables and vegetation function proxies to evaluate the capacity of atmosphere inverse models (AIMs) in characterizing the IAV of NEP at both the continental scale and subregional scales using correlation analyses. Finally, we choose the core areas impacted by the drought events in 2012 and 2015, and we assess the reasonability of AIMs for quantifying regional total annual anomalies and the seasonal anomalies of NEP. During the assessment, these environmental variables and vegetation function proxies are used as references, while the estimates from TRENDY models and FLUXCOM are used for comparison.

3. Results

3.1. Spatiotemporal Anomalies of Environmental Variables and Vegetation Function During 2001–2015

The anomalies of hydrological indicators (Prep, SM, and VPD) and vegetation variables (CSIF and NIRv) revealed several drought events in Europe, mainly during summer time (Figure 1a). Considering mainly based on the anomalies of precipitation and SM, together with suppressed vegetation activity, the droughts in 2003, 2006, 2012, and 2015 were chosen for analysis. These drought (and/or heatwave) events have been reported previously (Ciais et al., 2005; Laaha et al., 2017; Peters et al., 2018; Teuling et al., 2010; Zahradníček et al., 2015). With respect to the magnitude of hydrological anomalies (Figure 1a), the 2003 drought was the severest one, followed by the droughts in 2006, 2012, and 2015.

Figure 1b shows the spatial patterns of drought impacts revealed by meteorological, hydrological, and vegetation metrics in these drought years. In general, strong negative hydrological anomalies (e.g., in SM) generally corresponded to large positive anomalies in air temperature (Ta) and VPD, and vice versa. Precipitation and SM exhibited generally consistent anomalies in the regions influenced by droughts, coinciding well with the impacted pattern on vegetation function indicated by the changes in CSIF and NIRv, for example, most of Europe in 2003, North Europe in 2006, South Europe in 2012, and Central and East Europe in 2015. The summer anomalies of GPP estimated by FluxSat and GOSIF showed similar patterns (Figure S2a in Supporting Information S1). Overall, the drought in 2003 was the largest with respect to drought extent and severity (pixels with large negative *Z*-score values), followed by the 2006 and 2015 droughts. It is worth noting that the 2012 drought was more southern than the others. These droughts largely affected non-forest ecosystems, that is, croplands in western, central, and eastern Europe and grasslands in southern Europe, which are often more vulnerable to droughts and regarded as the major ecosystems dominating the IAV of regional land carbon uptake (He, Ju, et al., 2018).

3.2. Inter-Annual Variations of Terrestrial Carbon Uptake Estimated by AIMs

3.2.1. Continental Scale

First, we examined the full 2001–2015 period for the global AIMs assimilating surface CO_2 data. Figure 2a shows the IAV of NEP in Europe estimated by a set of global AIMs over 2001–2015. These classic global AIMs (CT, CTE, CAMS, and Jena) showed quite divergent IAV of NEP and in some years even anomalies with opposite signs (e.g., in 2003 and 2006). These global AIMs inconsistently captured the expected negative impacts of drought on NEP in years including 2003, 2006, and 2012, but not in 2015. In comparison, the inversions by Jena NEE–T

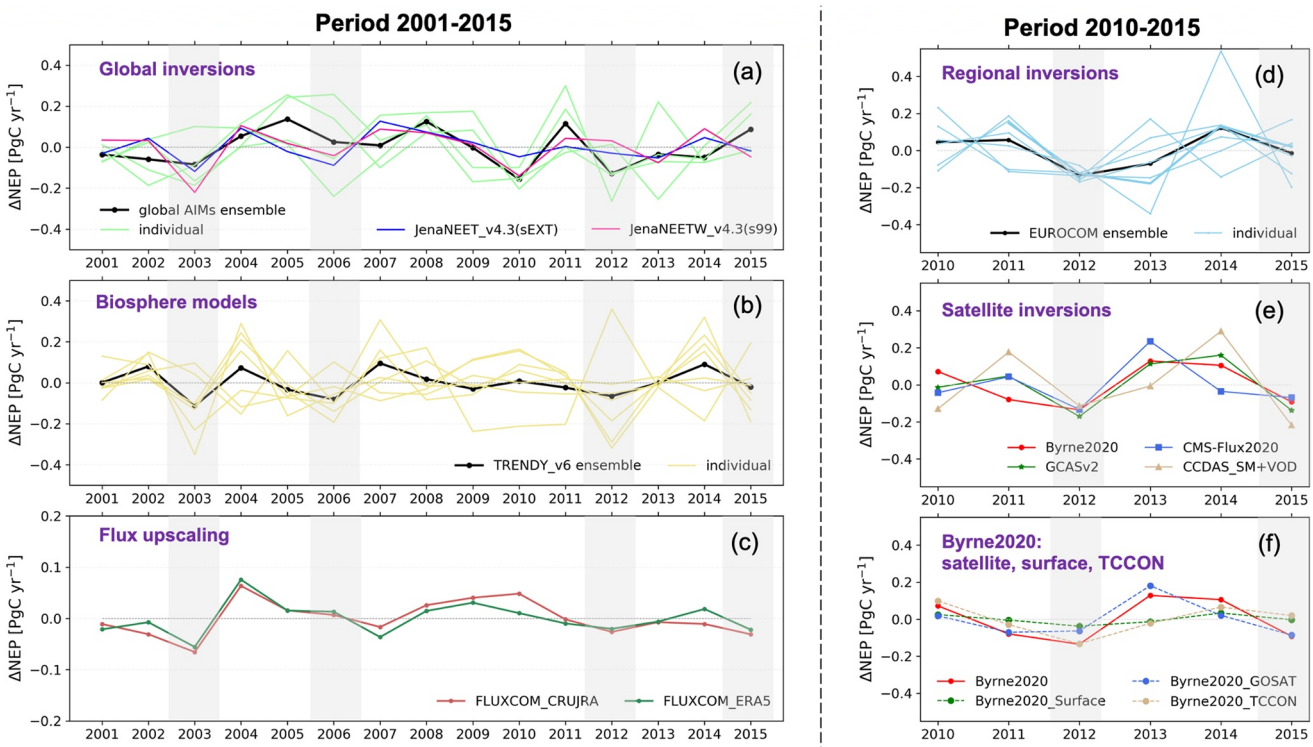

Figure 2. Annual net ecosystem production (NEP) anomalies estimated by global in situ CO_2 based global Atmospheric CO_2 inverse models (AIMs), EUROCOM in situ based regional AIMs, satellite-based AIMs, the TRENDY models, and FLUXCOM over 2001–2015 or 2010–2015. The shallow green shaded band in the bottom plot stands for the mean plus/minus the standard deviation for the NEP anomaly.

and Jena NEE–T–W, in conjunction with the ensemble mean NEP of TRENDY models (Figure 2b), identified the four drought years (2003, 2006, 2012, and 2015), which roughly agreed with the timing of satellite-based land surface variables (see Figure 1a, Figure S2b in Supporting Information S1). The FLUXCOM RS + METEO estimates, driven either by CRUJRA and ERA5, captured drought years, like 2003, 2012, and 2015 (Figure 2c). However, large discrepancies were found among atmospheric inversions and bottom-up estimates by TBMs or flux upscaling, and drought-induced NEP anomalies cannot be robustly captured for all cases.

We now focus on the 2010–2015 period (Figures 2d–2f), which is covered by all AIMs examined here. This period contains the two drought years of 2012 and 2015. In these two years, the TRENDY model ensemble mean NEP, the FLUXCOM RS + METEO NEP estimates, as well as both FluxSat and GOSIF GPP, exhibited negative anomalies (see Figures 2b and 2c, Figure S2b in Supporting Information S1). In contrast, the AIMs assimilating only surface CO_2 measurements showed a large spread between models for both 2012 (range: −263.71 to 13.32 TgC/yr) and 2015 (range: −15.87 to 217.18 TgC/yr). However, the AIMs applied regression relationships with temperature and water stress data, that is, Jena NEE–T (−18.69 TgC/yr) and Jena NEE–T–W (−47.75 TgC/yr), also showed a negative anomaly in 2015 (Figure 2a). The EUROCOM regional inversions all captured a consistent reduction in NEP during 2012 (range: −169.57 to −80.47 TgC/yr) (Figure 2d). However, these inversions showed divergent estimates for other years, and did not capture an NEP reduction for 2015 (range: −197.57 to 166.67 TgC/yr). Finally, the satellite-based inversions (Byrne2020, CMS-Flux2020, GCASv2, and CCDAS) captured the reduction in NEP by both the 2012 (range: −170.32 to −112.88 TgC/yr) and 2015 (range: −218.00 to −91.85 TgC/yr) droughts (Figure 2e). We further found that the inclusion of satellite XCO_2 measurements was critical for capturing the drought-induced NEP reductions for the Byrne2020 flux inversions, as a set of inversion that only assimilated the surface in situ data were unable to capture the negative anomaly in 2015 (Figure 2f).

To evaluate the robustness of the IAV indicated by these global inversions, regional inversions, and satellite inversions, we calculated the correlation coefficients between the IAVs of estimated NEP by these models and environmental variables and covariates (Figure 3). We found that the IAVs in Jena NEE–T and NEE–T–W, some regional inversions (e.g., EnKF-RAMS, FLEXINVERT, CarboScope-Regional, and NAME-HB), and satellite

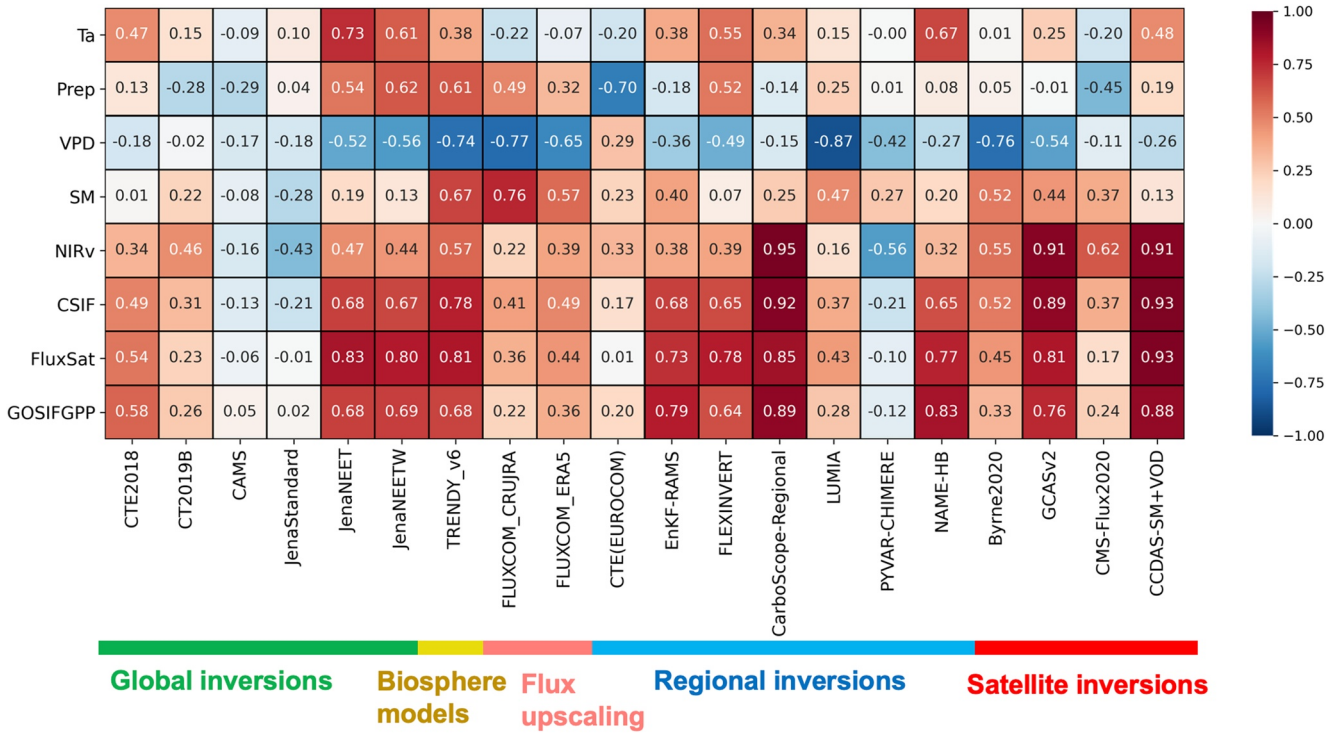

Figure 3. Heat map of the correlation between environmental variables and estimated net ecosystem production by global Atmospheric CO_2 inverse models (AIMs), EUROCOM in situ based regional AIMs, satellite-based AIMs, the ensemble mean of TRENDY models, and FLXUCOM.

inversions (e.g., GCAS v2 and CCDAS_SM + VOD), as well as the TRENDY model ensemble mean, highly correlated with the IAVs of most environmental variables and covariates, indicating the good representation of IAVs for these NEP estimates. Among global AIMs using only in situ CO_2 observations, CTE2018 correlated with environmental variables mostly strongly, which could be resulted from more in situ CO_2 observations assimilated over Europe and the higher model resolution in the domain of Europe in comparison to other global inversions. We also noticed some inversions, for example, CAMS, Jena Standard, and PYVAR-CHIMERE, show very low or even negative correlations with environmental variables and covariates, which may indicate a low capacity in constraining the NEP IAV over the continental scale of Europe. In addition, the IAVs in Jena NEE–T and NEE–T–W, the TRENDY model ensemble mean, and FLUXCOM estimates trained with meteorological data, show a high correlation with that of precipitation, while it is not so for most regional inversions and all satellite inversions, which may indicate an overestimated sensitivity to precipitation for these models directly constraining the IAV of NEP with meteorological data.

To further understand the role of observational constraints used for the AIMs in uncovering drought-induced NEP reductions, we examined the performance of their prior fluxes in capturing drought impacts (Figures S3 and S4 in Supporting Information S1). Effective constraints can be found in these posterior estimates. Here we took the regional inversions and satellite inversions as examples. Previous studies have shown that prior IAV applied in inversion systems can strongly impact posterior IAV estimates (Byrne et al., 2019), thus it is important to examine the impact of these prior constraints on flux estimates. The prior NEP estimates for the EUROCOM regional AIMs generally did capture the NEP reductions in 2012 and 2015. For 2012, the prior spread (range: −251.03 to 56.64 TgC/yr) was clearly larger than the optimized fluxes (range: −169.57 to −80.47 TgC/yr), suggesting that the AIMs were better able to capture this event than the prior fluxes. However, for 2015, the prior fluxes showed a more consistent reduction in NEP (range: −150.52 to 8.52 TgC/yr) than the optimized fluxes (range: −197.57 to 166.67 TgC/yr). Thus, the assimilation of CO_2 measurements generally resulted in large changes in NEP anomalies for the EUROCOM AIMs, however, the impact of these data was not always consistent between models. For the AIMs assimilating satellite data, we found that the priors generally did not capture the drought impacts (except that the GCAS prior captured reduced NEP in 2012, note Byrne2020 did not employ prior IAV). This suggests that the AIMs obtained consistent posterior NEP reductions for 2012 and 2015 despite the fact that

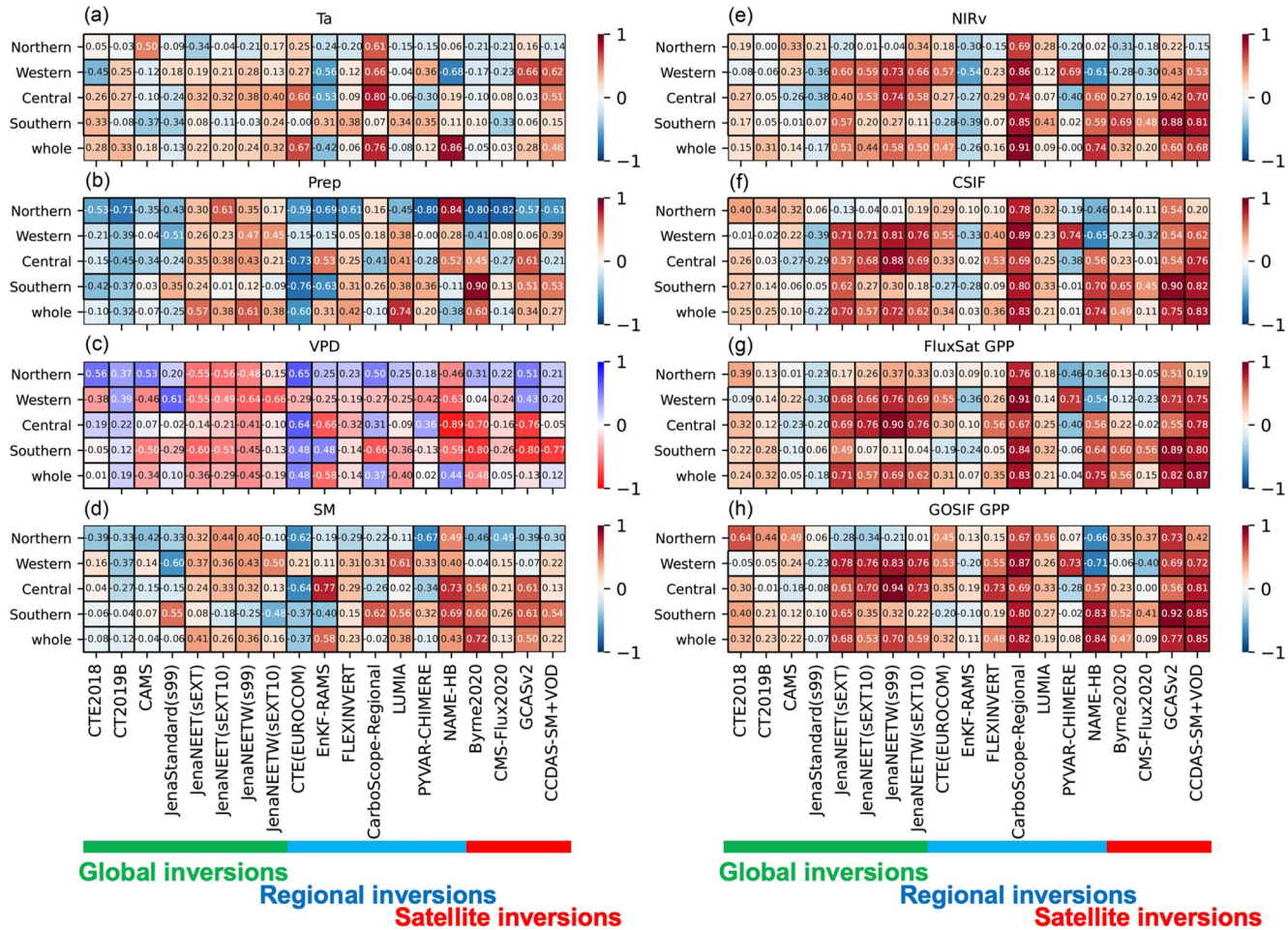

Figure 4. Correlation between the anomalies in the ensemble mean of TRENDY models or contiguous solar-induced fluorescence and annual net ecosystem production estimated by Atmospheric CO_2 inverse models (in situ based global inversions, EUROCOM regional inversions, and satellite-based inversions) across the four subregions. The Jena NEE-T and NEE-T-W inversions have several versions: sEXT indicates the inversion included in situ observations of global 87 stations by default, and sEXT10 indicates the inversion additionally included most recently in situ observations since 2010.

these events were generally not well captured by the prior fluxes. This result gives increased confidence in the ability of these systems assimilating satellite data to uncover drought-induced reduction in NEP over Europe.

3.2.2. Subcontinental Scale

We further looked into the ability of AIMs in tracking the IAV of NEP across different regions (defined in Figure S1b in Supporting Information S1). We analyzed the correlations between the IAVs in the inverted NEP fluxes by inversions and the IAVs in environmental variables and covariates (Figure 4). The IAV in FluxSat and GOSIF GPP showed significant correlations with the IAVs in most environmental variables (e.g., Ta, Prep, SM, and VPD) and vegetation functions (e.g., NIRv and CSIF) (see Table S5 in Supporting Information S1), thus we expect that the AIMs to show some consistency with the IAVs of these environmental variables and covariates on subcontinental scales.

First, we analyzed the correlations between annual NEP from in situ based global AIMs and that from the environmental variables and covariates across the four subregions. We found that the in situ based global inversions were generally in low correlation with the environmental variables and covariates. However, there were exceptions, Jena NEE–T and Jena NEE–T–W inversions, for which the performances in most of the four subregions and the entire area showed much stronger correlations. Compared with the Jena standard inversion, these inversions with additional constraints from surface variables (temperature or/and water) largely increase the correlation with environmental variables and covariates. This could be an important improvement, which means the surface variables

add useful information that enables AIMs to reflect more detailed spatial patterns. In comparison, the correlations with most environmental variables and covariates were quite low in the northern region and the southern region, even for these Jena NEE–T and Jena NEE–T–W inversions, which may indicate low confidence in constraining NEP IAV in these regions due to limited in situ CO_2 observations. When looking at the correlations with vegetation variables, this phenomenon is even more obvious.

Then, we analyzed the correlations between annual NEP from regional inversions constrained by enhanced in situ CO_2 observations or global inversions constrained by satellite data and that from the environmental variables and covariates across the four subregions. Stronger correlations were found between these regional or satellite inversions and the environmental variables and covariates for these different subregions, typically in the western, central, and southern Europe, and the correlations reached as high as 0.91 (between NIRv and CarboScope-Regional) for the whole area. Some regional inversions (e.g., FLEXINVERT, CarboScope-Regional, and NAME-HB) and satellite-based inversions (e.g., Byrne2020 and GCASv2) had a comparable performance with the Jena NEE–T and NEE–T–W inversions. One clear difference was that the Jena NEE–T and NEE–T–W inversions had stronger correlations with environmental variables (e.g., Prep, VPD, and SM) for northern Europe while the regional and satellite-based inversions did not correlate as strongly. In comparison, the latter had stronger correlations in southern Europe where the Jena NEE–T and NEE–T–W inversions did not. To make sure the improvement in tracking IAV of NEP is from observations but not from the priors, we also checked the correlation between the AIMs priors and the environmental variables and covariates (Figure S5 in Supporting Information S1). The results show that the priors are more strongly correlated with the environmental variables and covariates, which may associate with that the priors are taken from biosphere models that are driven directly by climate variables. After constraining with enhanced surface CO_2 observations, the correlation reduction means that observations take effect and the correlation by the prior could have been overestimated. Overall, the correlation analysis with different variables showed a similar pattern, with a clearly higher correlation with GPP and its proxies (i.e., NIRv, CSIF) than environmental variables (i.e., Ta, Prep, VPD, and SM). One noticeable common low correlation among all variables was found in northern Europe, which may be explained by the difficulty for these inversions to capture relatively mild IAV with limited CO_2 observations over there. We also noticed some negative or very low correlations with GPP and its proxies in different regions, which may indicate a limited capacity of the inversions in constraining NEP IAV in these regions or physical reasons for why NEP should not necessarily correspond to GPP, e.g., if respiration fluxes have offsetting effects.

Furtherly, we analyzed the improvement in the correlations between the optimized NEP fluxes of global AIMs, EUROCOM regional inversions, and satellite-based inversions) and the ensemble mean of environmental variables and covariates in comparison to prior estimates (Figure S6 in Supporting Information S1). We found substantial improvements in the correlations in optimized fluxes compared to those in priors for the satellite-based inversions (Figures S6b and S6d in Supporting Information S1), while most priors in EUROCOM inversions have better correlations than posteriors (optimized fluxes). In some way, this means the surface CO_2 observations used for EUROCOM are still insufficient if we are expected to constrain carbon flux estimates at the subcontinental scale.

3.3. Regional Analysis of Drought Impacts on Terrestrial Carbon Uptake Revealed by AIMs

We investigated the NEP anomalies estimated by different AIMs in the selected drought-impacted regions (shown in Figure 1b) in 2012 and 2015 in comparison to those of the TRENDY model ensemble and the FLUXCOM estimates (Figure 5). For 2012, we found ensemble mean NEP anomalies of −49.74 PgC/yr for the global surface CO_2 AIMs, −149.73 TgC/yr for EUROCOM regional AIMs, −80.18 TgC/yr for the AIM_S with space-based constraints, −130.72 TgC/yr for the TRENDY model ensemble mean, and an average of −38.35 TgC/yr for the two FLUXCOM estimates. For 2015, we found ensemble mean NEP anomalies of +37.91 TgC/yr for the global surface CO_2 AIMs, +39.70 TgC/yr for EUROCOM regional AIMs, −104.65 PgC/yr for the AIM_S with space-based constraints, and −31.71 TgC/yr for the TRENDY model ensemble mean, and an average of −17.20 TgC/yr for the two FLUXCOM estimates. Although a large spread of the magnitudes of flux anomaly across AIMs existed, the global inversions constrained by both in situ CO_2 and ancillary data (i.e., Jena NEE–T and NEE–T–W), some in situ based regional inversions (e.g., CarboScope-Regional and LUMIA), satellite-based inversions, the TRENDY model ensemble mean, and the two FLUXCOM estimates captured reduction in NEP in the two drought years. Overall, these models pointed to a negative sign of flux changes in 2012. Most in situ based global inversions failed to capture the negative sign of flux changes in 2015. However, the Jena NEE–T and NEE–T–W inver-

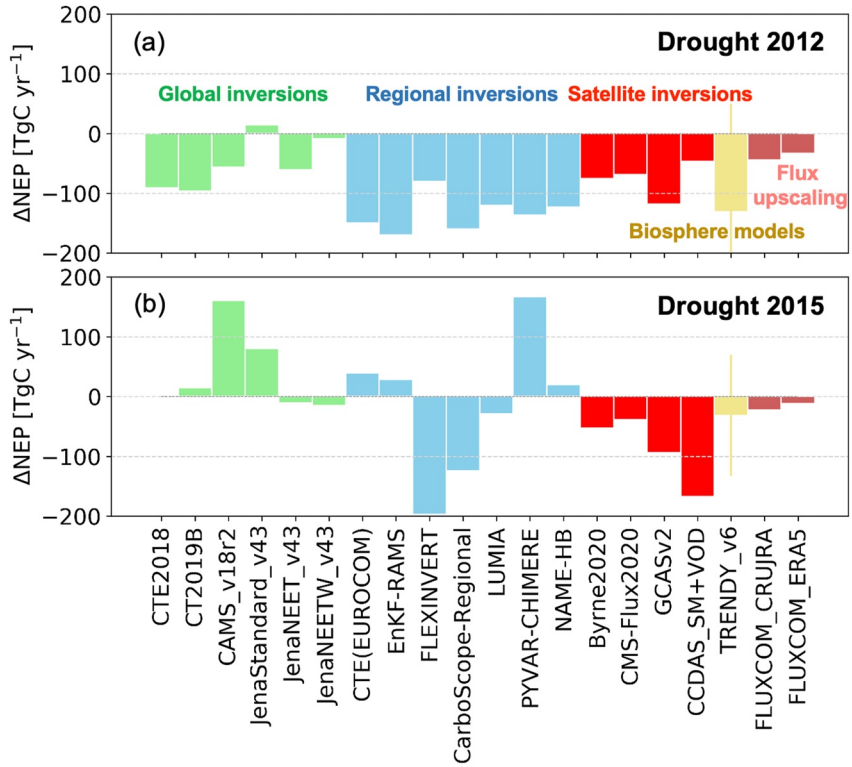

Figure 5. Annual net ecosystem production anomalies estimated by in situ based global inversions, EUROCOM in situ based regional Atmospheric CO_2 inverse models (AIMs), satellite-based AIMs, the TRENDY models, and FLXUCOM in the selected drought-impacted regions in 2012 and 2015 as indicated in Figure 2. The error bar for the TRENDY models indicates one standard deviation.

sions did show a negative flux anomaly though very small. The optimized fluxes of the in situ based regional inversions demonstrated some improved consistency in capturing the total flux anomalies compared to those in priors (Figure S7a in Supporting Information S1). For example, the uncertainty for a flux reduction in 2012 was reduced obviously, with the standard deviation reduced from 84.6 TgC in the priors to 27.7 TgC in the posteriors. Similarly, the optimized fluxes of the satellite-based inversions showed substantial improvements compared to those in priors (note Byrne2020 did not employ prior IAV), for example, the GCASv2 prior indicated an opposite direction of flux anomaly (carbon uptake increase) in 2015 compared with others, but after optimization, all these inversions indicated the carbon uptake reduction (Figure S7b in Supporting Information S1).

We further analyzed the seasonal anomalies of carbon fluxes according to meteorological, remotely sensed hydrological, and vegetation variables in the drought-impacted regions over the two drought years (Figure 6). For 2012, most EUROCOM regional inversions and satellite-based inversions (except for CCDAS) appeared a double-valley of NEP anomalies, which was similar to those indicated by the TRENDY model ensemble (Figure 6d), FLUXCOM (Figure 6e), NIRv and CSIF (Figure 6i) and two GPP data sets (Figure 6j). In addition, the optimized fluxes of the satellite-based inversions were quite consistent in capturing the seasonal anomalies and agreed better with EUROCOM regional inversions and bottom-up estimates (i.e., by TRENDY and FLUXCOM) compared to those in priors (Figure S8b in Supporting Information S1). In contrast, the in situ based global inversions showed large model-to-model differences in the NEP anomalies over 2012, which were also largely different from those of in situ based regional inversions and satellite-based inversions. This suggests that the assimilated CO_2 observations in these global AIMs were insufficient to uncover the regional NEP anomaly. Similarly, for 2015, there was good consistency in the seasonal anomalies between the EUROCOM regional inversions, the TRENDY model ensemble mean (Figure 7n), FLUXCOM (Figure 7o), NIRv and CSIF (Figure 7s), and GPP data sets (Figure 7t). In particular, all data sets showed a maximum reduction in August. However, the global in situ inversions generally showed divergent NEP anomaly estimates (Figure 7k). Also, the ensemble mean of EUROCOM optimized fluxes exhibited clearly more reasonable seasonal anomalies of carbon fluxes, that is, spring enhancement followed by summer reduction (Figure 7i), in 2015 than that of prior fluxes (Figure S8c in Supporting Information S1)

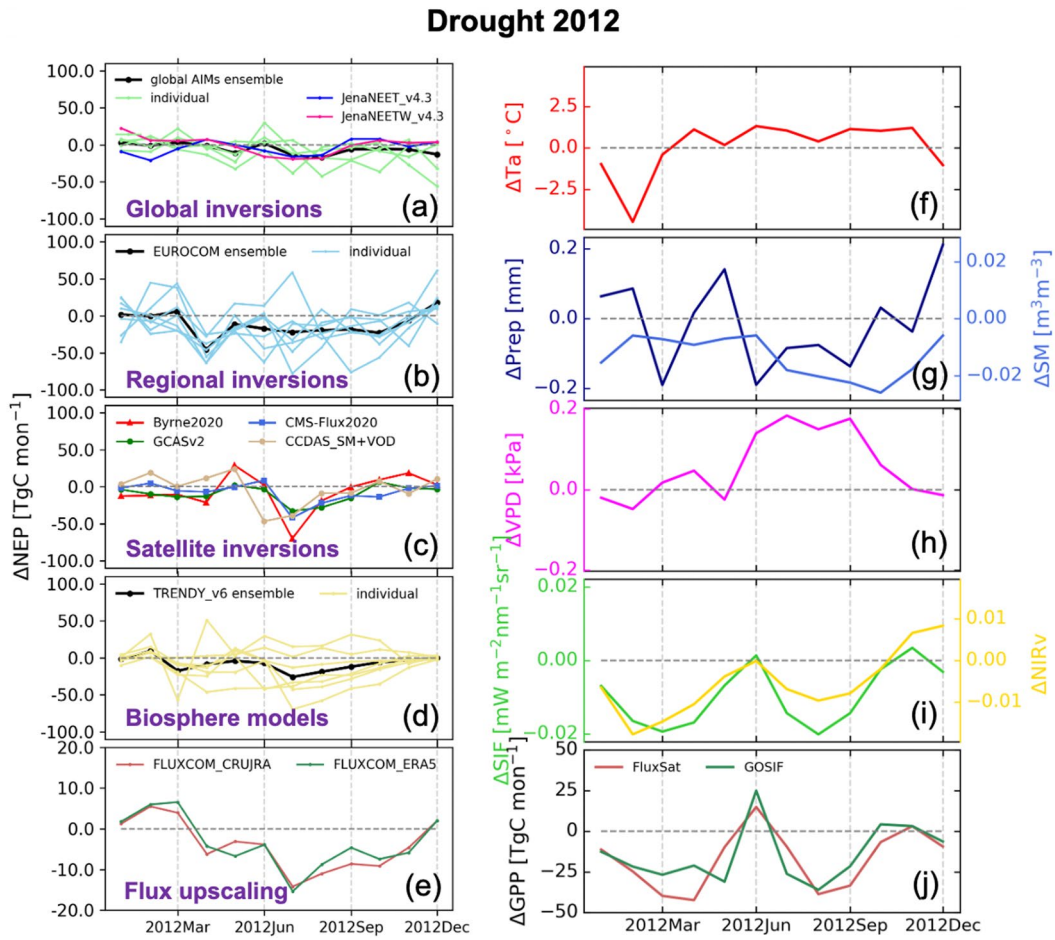

Figure 6. Seasonal anomalies of net ecosystem production estimated by an ensemble of in situ based global Atmospheric CO_2 inverse models (AIMs), EUROCOM regional AIMs, satellite-based AIMs, the TRENDY models, and FLUXCOM, and seasonal anomalies of corresponding hydroclimate and vegetation variables for the selected drought-impacted regions in 2012.

considering the corresponding seasonal meteorological anomalies. It is worth noting that the seasonal redistribution phenomenon (Butterfield et al., 2020; Wieder et al., 2021) in 2015 as mentioned above is well captured by the EUROCOM ensemble mean, which is in line with those in the TRENDY ensemble mean and FLUXCOM. In addition, the optimized fluxes of the satellite-based inversions (Figure 7m) clearly showed improvements in capturing the seasonal anomalies compared to their priors, for example, the priors of most inversion models failed to capture uptake reduction during the drought (Figure S8d in Supporting Information S1). It should be noted that the seasonal anomalies of satellite-based inversions do not outperform in situ based global inversions and regional inversions. For example, in 2012, satellite-based inversions do not show a double valley of NEP anomalies; in 2015, three of four satellite-based inversions show large positive anomalies in July, which are not consistent with other estimates. These indicate there is still space for further improvements in satellite-based inversions.

In order to further verify the revealed seasonal anomalies, we investigated the seasonal variations of NEP in 2012 and 2015 using eddy covariance measurements (Figure 8). Crop/grass showed clearly stronger seasonal anomalies than forest did in both years. These measurements in 2015 showed consistent anomalies as those in the remotely sensed variables, while not in 2012, due to the very limited available flux sites in eastern and southeastern Europe where the 2012 drought mainly impacted. In 2015, spring warming slightly increased NEP, which partly offset the loss during the following summer drought. This kind of seasonal compensation has also been found in eastern North America (Byrne, Liu, Bloom, et al., 2020) and in the 2012 North American drought (He, Ju, et al., 2018; Wolf et al., 2016) and the 2018 European drought (Smith et al., 2020; S. Wang et al., 2020).

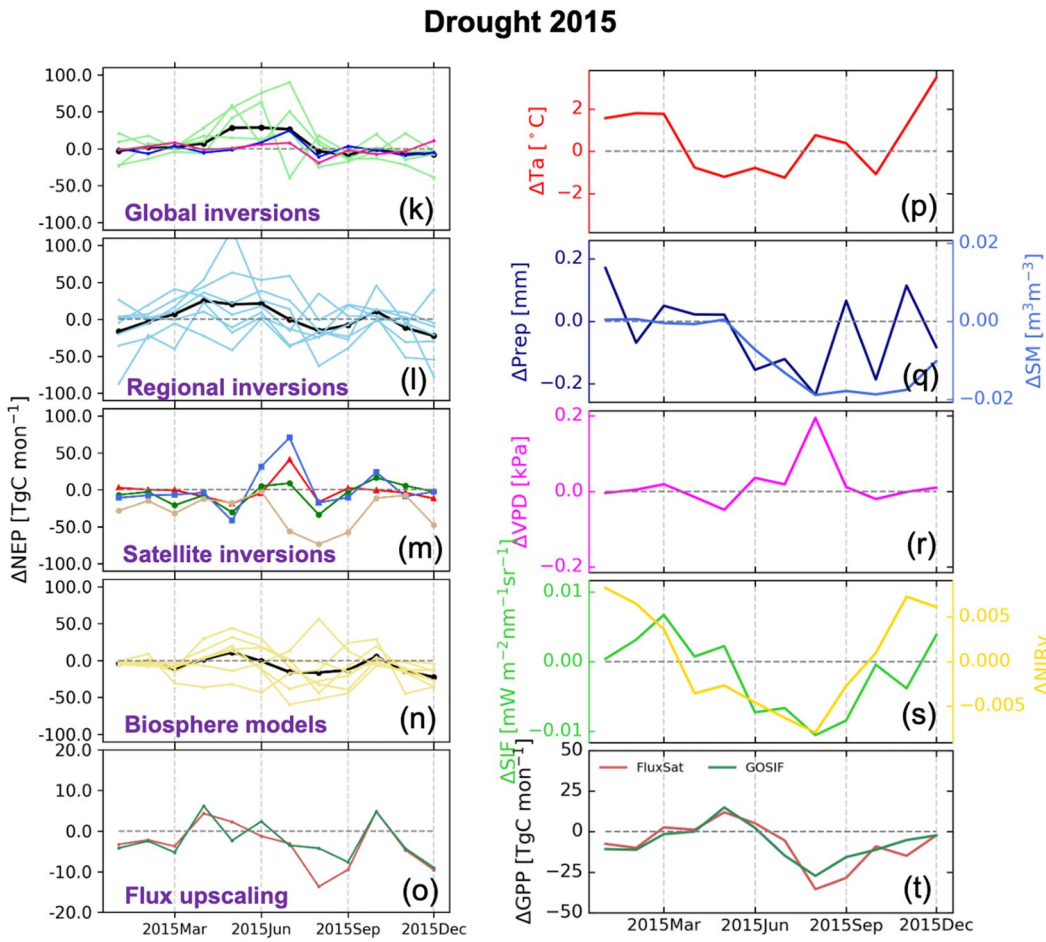

Figure 7. Similar to Figure 6, but for the drought 2015.

In addition, we investigated which land cover types within the selected regions were dominantly affected by the droughts in 2012 and 2015. The regions were selected according to the anomalies in VPD and SM (Figure 1b). Here the MODIS landcover was used as the base map for the statistics. For 2012, the top three dominant land covers are barren or sparsely vegetated (20.83%), crops (11.61%), and grasslands (7.33%); in 2015, the top three land covers are crops (31.11%), mixed forests (20.46%), and cropland or natural vegetation mosaic (12.46%). In both years, a large portion of drought areas was covered by crops or grasses, which contributed to the large negative flux anomalies. In the year 2015, the considerable amount of forest increased carbon uptake during warm spring, which compensated for carbon loss in the following summer. For 2015, the impacted area of crops and relative types outweigh that of forests, thus the annual NEP was likely reduced, which was consistent with the estimates by partial in situ based global inversions (Jena NEE–T and NEE–T–W) and EUROCOM regional inversions (i.e., FLEXPART, CarboScope-Regional, and LUMIA), satellite-based inversions, the TRENDY ensemble mean, and the FLUXCOM RS + METEO estimates (see Figure 7).

3.4. Detected Recent Droughts by OCO-2 XCO_2 Inversions

The recently available OCO-2 XCO_2 inversions provide a great chance to examine the capacity of satellite XCO_2 inversions on detecting the impact of droughts that occurred since 2015 on the European land carbon sink. We conducted some analyses using the more recent satellite inversions with OCO-2 XCO_2 retrievals, namely OCO-2 v10 MIP (Byrne et al., 2023; more details about the inversion models refer to Table S6 in Supporting Information S1) and the GGAS OCO-2 inversion (Jiang et al., 2021), to investigate the recent droughts in 2015 and 2018. Both the ensemble median of OCO-2 v10 MIP inversions and the GGAS OCO-2 inversion successfully detected the carbon sink reductions in 2015 and 2018 caused by large-scale drought impacts, albeit with considerable inter-model discrepancies, while not well captured by their prior estimates (Figure 9).

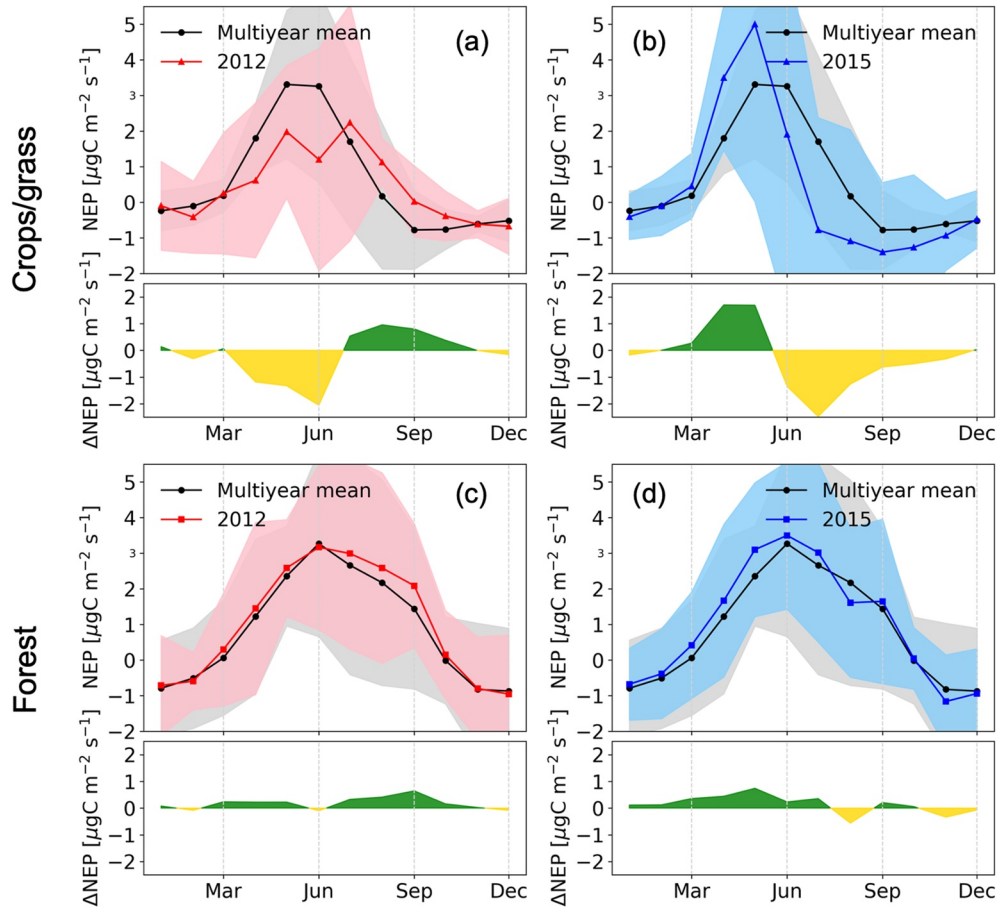

Figure 8. Seasonal variations of net ecosystem production in 2012 and 2015 based on eddy covariance measurements. The mean flux of 10 crop/grass sites (6 crop sites and 4 grass sites) and that of 9 forest sites (6 ENF sites and 3 DBF sites) were calculated, respectively. A same group of eddy flux sites roughly located in the impacted area by the two events (total of 19 sites) was chosen for the analyses, where these sites better represent the impact by the 2015 event. Note that the land cover type is characterized by the actual landcover reported in each site. The shallow bands indicate one standard deviation.

We chose the 2015 drought and the 2018 drought to further analyze seasonal anomalies (Figure 10). The inversions revealed clear seasonal dynamics for both drought years while their prior estimates did not. The seasonal climate conditions of the two droughts have been well-documented by previous studies (Smith et al., 2020; Thompson et al., 2020). The 2015 drought has a similar seasonal climate feature as the 2018 drought, namely, a spring warming followed by a summer drought. The OCO-2 inversions show slight advantages in indicating the spring NEP enhancement in 2015, moreover, they are able to track the impact of the 2018 spring warming and summer drought very well. Compared with the 2015 drought, the 2018 drought was better detected in seasonal anomalies, possibly due to the much larger drought scale for the 2018 event and the impact on the ecosystem carbon sink is much severer. In principle, stronger carbon sink anomalies can be easier to be detected by satellite signals.

4. Discussion

4.1. Benefits of Increasing In Situ CO_2 Observations to Capturing Regional Drought Impacts

The global inversions based on only limited surface CO_2 data generally face difficulties in reflecting regional drought impacts on terrestrial carbon uptake, which is in line with the findings of Byrne et al. (2019) and E. Lee et al. (2020). This originates from the sparse network of CO_2 observations used for constraining carbon fluxes, which do not provide sufficient information to precisely constrain subcontinental CO_2 flux anomalies. Encouragingly, the recent developing regional inversions with enhanced surface CO_2 observations by the EUROCOM project better capture the drought-induced carbon uptake reduction for 2012 relative to the common global inver-

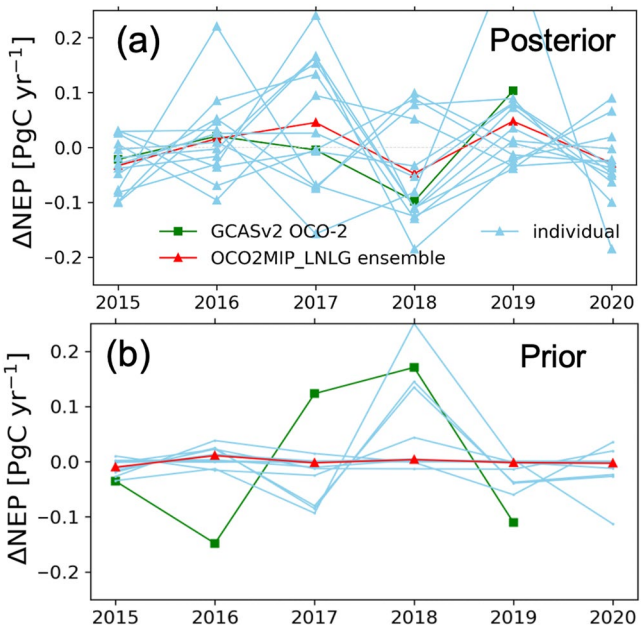

Figure 9. Annual net ecosystem production anomalies over Europe estimated by the GCASv2 OCO-2 inversion and OCO-2 v10 MIP (a) during the period 2015–2020 in comparison to prior estimates (b). Although large inter-model discrepancies existed, the posterior flux estimate captured the drought impacts in 2015 and 2018 while the prior did not.

sions, however, these inversions also show some deficiencies. In particular, the EUROCOM inversions show a large spread in NEP anomalies for most years and do not consistently capture a reduction in NEP for 2015.

Several recent studies provide extra evidence for the importance of increasing CO_2 observational coverage for capturing drought impacts. For the CTE inversion system, it showed no drought response of the European carbon uptake in the 2018 summer with the default CO_2 data (around 10 stations) as used for global purposes, but it showed drought response when including extensive surface CO_2 data (in total 48 stations) in Europe (Smith et al., 2020). Similarly, the Jena CarboScope s10 inversion performed better in capturing the 2018 European drought impact than the s99 inversion due to the additional CO_2 stations (Rödenbeck et al., 2020). These indicate that increased CO_2 observations are critical for constraining anomalies in carbon fluxes at subcontinental scales.

Despite the recent expansion of the network of surface CO_2 measurements, we find that there are still difficulties for in situ based regional inversions to accurately track seasonal anomalies of carbon fluxes in 2012 and 2015. This is likely partially due to an uneven distribution of sampling locations, with the sparse surface CO_2 observations in the drought-impacted regions in eastern Europe (see Figure S1b in Supporting Information S1). More surface CO_2 observations, especially in eastern Europe, are critically needed for better constraining the subcontinental scale carbon fluxes. As climate-sensitive regions, the south and the central east areas dominated the IAV of NEP in Europe, but these areas did not have as many observations as the central west region; more attention needs to be paid to the south and central east areas in the future.

A notable finding of this work is that EUROCOM ensemble models show a large spread in inverted fluxes. This demonstrates the sensitivity of individual flux inversions to aspects of the inversion set-up, such as the choice of prior fluxes and the specification of their uncertainties, lateral boundary conditions, transport models, and the design of optimization schemes (i.e., what variables are exactly optimized). This further motivates the use of flux inversion ensemble experiments to more fully characterize uncertainties in posterior flux estimates.

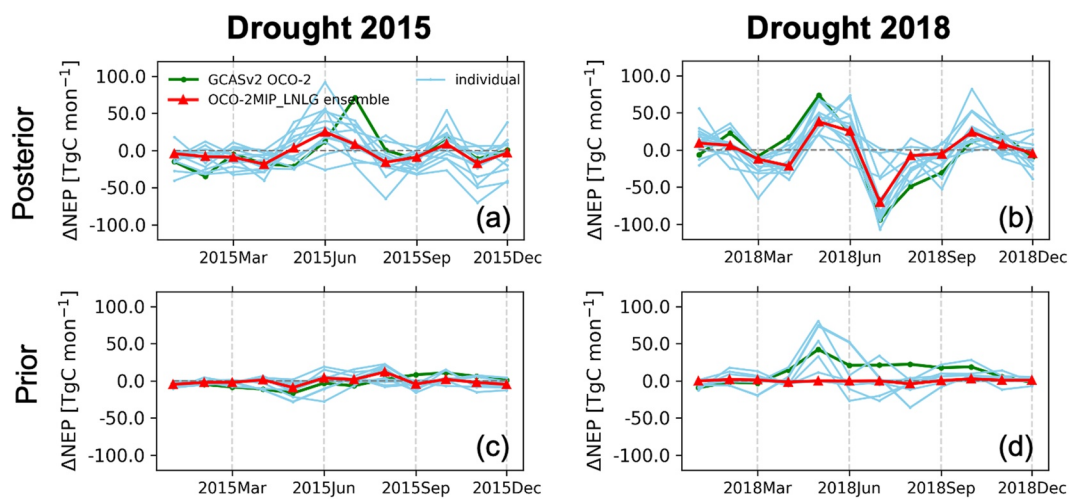

Figure 10. Seasonal anomalies of net ecosystem production during the drought years of 2015 and 2018 estimated by the GCASv2 OCO-2 inversion and OCO-2 v10 MIP (a, b) in comparison to prior estimates (c, d).

4.2. Importance of Satellite XCO_2 for Capturing Regional Drought Impacts

The global inversion that assimilates satellite XCO_2 data in addition to in situ CO_2 data also indicate an improved ability to capture flux anomalies at subcontinental scales. For example, the Byrne2020 inversions which assimilated GOSAT XCO_2 data reasonably capture the reduction of carbon uptake in 2015, while unable to do so when assimilating only in situ CO_2 data (see Figure S4 in Supporting Information S1). Although the prior flux prescribed in the Byrne2020 inversion did not contain any interannual anomalies, the posterior flux reproduced the right pattern of drought-induced NEP reductions. Similarly, for GCASv2, with the constraint from GOSAT XCO_2, the posterior flux usefully uncovers the NEP reduction in 2015 (Figure S4 in Supporting Information S1). Most encouragingly, with the constraint of satellite XCO_2, the different inversion systems reached a convergence for indicating drought impact at the regional scale of Europe (Figure 2e), and improved consistency with the inversion estimates from EUROCOM, Jena NEE–T and NEE-T-W, and CCDAS compared to their priors. These satellite inversions also largely improve the correlations with environmental variables and vegetation functions (Figure S6 in Supporting Information S1).

Compared to in situ CO_2 observations, satellite XCO_2 provides better data coverage and improved spatial representativeness, which could largely contribute to the improvement of drought-impacted carbon flux detection. That is because, data coverage and spatial representativeness are always important aspects determining the capacity of atmospheric inverse modeling to reveal fine-scale spatial patterns, where trade-offs between adjacent regions often happen if there are insufficient constraints (Peylin et al., 2013). A few studies have also reported successful applications of satellite XCO_2 based inversions for assessing climate extreme impacts on terrestrial carbon fluxes (Byrne et al., 2019; Ishizawa et al., 2016; Kwon et al., 2021; J. Liu et al., 2017, 2018; Yin et al., 2020). Complemented with them, we confirmed the advantages of utilizing satellite XCO_2 in atmospheric inverse modeling for monitoring regional climate extreme impacts.

It should be noted that some deficiencies existed in the XCO_2 inversions for drought impact monitoring, for example, the inversions did not reasonably reproduce the full seasonal anomalies, for example, failed to indicate a likely enhancement of NEP in the spring of 2015 (See Figures 6 and 7). One possible reason for explaining this could be that the inverted fluxes are less constrained at the early glowing season due to less data coverage than that at peak growing season in Europe (as illustrated by Jiang, He, et al. (2022) and Ishizawa et al. (2016)). In addition, satellite-based inversions like Byrne2020 and CMS-Flux2020 seem to perform not as well as regional inversions and Jena inversions in Western Europe where a dense network of in situ measurements exists, which may associate with the coarse model resolution used ($4° \times 5°$ used for and Byrne2020 and CMS-Flux2020). These issues call for further investigations.

4.3. Importance of Ancillary Environmental Variables for Capturing Regional Drought Impacts

In our analyses, the inclusion of extra environmental constraints, such as moisture conditions (e.g., CCDAS) result in drought-induced NEP anomaly estimates that better agree with anomalies in environmental variables, remote sensing of vegetation, and the ensemble mean of the TRENDY models. In atmospheric inversions, critical environmental variables, either from meteorological reanalysis data or satellite land surface data, are able to better reveal drought impacts.

The CCDAS inversion with constraints from remotely sensed land variables is able to reasonably indicate drought-induced NEP reductions in both 2012 and 2015, yet not so in the prior simulated by TBM. The CCDAS flux estimates have also been effective in indicating environmental stresses in previous studies (He, Jiang, Wu, et al., 2022; Wu et al., 2020). Different from the way adopted by Jena inversions, CCDAS assimilates remote sensing data (e.g., SM, VOD, and FAPAR) in addition to in situ atmospheric CO_2 concentrations to constrain carbon fluxes through the optimization of underlying parameters in TBM. In CCDAS, the IAV of carbon fluxes could be improved through the information on nature variability contained in the land surface data, for example, SM and vegetation variables.

It is worth noting that there were still some deficiencies in the inversions for drought impact monitoring, for example, the CCDAS inversion did not reasonably reproduce the seasonal anomalies for example, failed to indicate a likely enhancement of NEP in the spring of 2015 (Figure 7), and likely overestimated the magnitude of drought-induced annual NEP reduction in 2015 (See Figure 5).

For the Jena NEE-T and NEE-T-W inversions, it is implemented in a different way. They applied extra constraints of surface temperature or plus SPEI obtained from meteorological reanalysis data, clearly outperforming the inversion using only atmospheric CO_2 data in characterizing IAV and impacts of extreme droughts on NEP. This advantage has also been documented in previous studies for impact assessments of the historical El Niño events (Rödenbeck et al., 2018a) and the 2018 European drought (Rödenbeck et al., 2020). They directly constrain the response of NEP to climate variations on inter-annual timescales by applying the relationship between inter-annual NEP anomalies and surface temperature or/and water anomalies to atmospheric inverse modeling. This operation clearly improved its performance for capturing climate impacts on NEP at regional scales.

4.4. Other Issues and Limitations

Recently, a collection of inversion studies (Peters et al., 2020) assessed the impact of the 2018 European drought and heatwave on the terrestrial carbon cycle. The collection mainly included the EUROCOM inversions (Thompson et al., 2020), a new version of CTE assimilated more observations and adapted with prior flux from the Simple Biosphere Model Version 4 that better-represented water stress (Smith et al., 2020), and the Jena NEE-T and NEE-T-W inversions (Rödenbeck et al., 2020). They successfully tracked the impact of the 2018 European drought and heatwave. In this study, we provided a more comprehensive evaluation of the capacity of current AIMs, both in situ based and satellite-based, in capturing drought impacts on ecosystem carbon uptake in Europe over the period 2001–2015. We additionally included satellite-constrained carbon flux estimates for investigations, and make the intercomparison of the different categories of inversion models in a unified analysis framework, which offers a useful perspective on the capacity of state-of-the-art atmospheric CO_2 inverse modeling for capturing regional drought impact on the European land carbon uptake.

In comparison to the 2012 drought, the 2015 drought impact seems to be more difficult to be well captured. This could be due to the effect of orography since it is centered around the Alps. Usually, modeling the atmospheric signals with transport models in mountainous area has higher uncertainties than in flat areas. Also, the seasonal compensation partially mitigated the impact, resulting in a much weaker carbon uptake reduction than a continuous reduction like the case of 2012. We also found for similar drought cases with seasonal compensation, the 2018 drought was clearly better detected in seasonal anomalies than the 2015 drought. We know that the 2018 event has a much larger impacted region and the impact on the ecosystem carbon sink is much severer. Compared to bigger drought events like the 2018 event, smaller ones like the 2015 event could be more difficult to be captured by inversion models.

Our analyses highlighted the importance of including satellite XCO_2 and ancillary environmental variables in the inversions for better uncovering regional carbon flux dynamics. In the future, the sustained development of satellite XCO_2 observations, such as OCO-2/3 (Kiel et al., 2021), GOSAT-1/2 (Suto et al., 2021), Tansat-1/2 (Y. Liu et al., 2018), GeoCARB (Moore et al., 2018), and CO_2M (Kuhlmann et al., 2020), would greatly benefit such purpose. The satellite-based land surface metrics, for example, SIF, SM, VOD, and other environmental variables, are pretty helpful for accurately charactering environmental stresses, serving for the evaluation of carbon cycle models toward precisely monitoring carbon dynamics especially under climate extremes as well as directly improving carbon flux simulations using data assimilation techniques (e.g., as the ways of Jena NEE-T and NEE-T-W, and CCDAS).

A limitation of our analysis is that the true NEP anomalies are unknown, and we are limited to using observations of environmental variability, measurements of vegetation function, and model estimates of NEP anomalies to investigate the performance of the AIMs. Therefore, the timing and magnitude of anomalies in these quantities likely have differences from the true NEP anomalies, such that differences between the AIMs and these quantities are likely due to a combination of errors in the AIMs and differences between these quantities and the true NEP anomalies. Still, recent studies have shown that we should expect to see a substantial correlation between these quantities and the AIMs during extreme events (Byrne et al., 2019; Yin et al., 2020), particularly in more moisture-limited ecosystems (Ahlström et al., 2015; Byrne, Liu, Bloom, et al., 2020). Therefore, the increased agreement of the EUROCOM regional models and space-based inverse models with the observations of environmental variability, measurements of vegetation function, and model estimates of NEP anomalies relative to the global in situ inversions provide strong evidence that these systems better capture drought-induced reductions in NEP. In addition, we encourage the further study if methods for evaluating the ability of AIMs to the impact of extreme events on NEP, in particular, methods that could better account for lagged impacts on ecosystems are encouraged.

5. Conclusions

We assessed the capacities of state-of-the-art AIMs in capturing drought impacts on the European land carbon uptake during the period 2001–2015. The assessment is made with both in situ based global or regional inversions and satellite-based inversions. The main findings are as follows:

1. Global atmospheric inversions with only limited surface CO_2 observations give divergent estimates of drought impacts on the European ecosystem carbon uptake;
2. A set of regional inversions assimilating a denser set of CO_2 observations over Europe, for the EUROCOM project, demonstrate some improved consistency among all inversions in capturing a reduction in carbon uptake during the 2012 European drought. However, the EUROCOM models show divergent estimates in interannual variability of carbon cycle uptake for most years;
3. A set of global inversion systems that assimilate satellite XCO_2 or land surface variables (e.g., SM and VOD for CCDAS) in addition to surface CO_2 observations better capture annual and seasonal anomalies of the European carbon uptake induced by regional droughts in both 2012 and 2015. In addition, the recent Orbiting Carbon Observatory—2 XCO_2 inversions captured the impacts of the 2015 and 2018 droughts, with better performances for characterizing the seasonal anomalies of the much larger-scale drought in 2018.

These results suggest that surface CO_2 observations may still be too sparse to fully capture the impact of drought on the carbon cycle at subcontinental scales over Europe, which calls for further expansion and optimization of surface CO_2 observation networks. Complemented to enhancing surface CO_2 observations, it is also of great importance to make full use of satellite XCO_2 or environmental variables in atmospheric inverse modeling. Further studies that assimilate satellite XCO_2 and ancillary environment data sets in addition to surface CO_2 measurements are warranted and offer a promising direction for refining estimates of regional carbon cycle anomalies.

Data Availability Statement

CTE2018 fluxes were obtained from the CarbonTracker Europe website (https://www.carbontracker.eu; Van der Laan-Luijkx et al., 2017). CT2019 fluxes were obtained from the CarbonTracker website (https://gml.noaa.gov/aftp/products/). CAMS_v18r2 fluxes were obtained from https://apps.ecmwf.int/datasets/data/cams-ghg-inversions/ (Chevallier et al., 2010) Jena CarboScope fluxes were obtained from http://www.bgc-jena.mpg.de/CarboScope/ (Rödenbeck et al., 2003). GCAS v2 carbon fluxes inferred from GOSAT and OCO-2 XCO_2 data are publicly available at https://doi.org/10.5281/zenodo.4500439 (Jiang, 2021) and https://doi.org/10.5281/zenodo.7040223 (He, Jiang, & Ju, 2022), respectively. OCO-2 v10 MIP fluxes are publicly available from https://www.gml.noaa.gov/ccgg/OCO2_v10mip/ (Byrne et al., 2023). NEE fluxes from Byrne, Liu, Lee, et al. (2020) are publicly available at https://data.nas.nasa.gov/carboncycle/co2flux/data.php. EUROCOM outputs were obtained from https://meta.icos-cp.eu/collections/6rMkbXz3W376i4lehBohpUox (Monteil et al., 2019). FLUXCOM (v2020) fluxes were obtained from http://www.fluxcom.org (Jung et al., 2020). Drought-2018 ecosystem eddy covariance flux product was obtained from the ICOS data portal (https://www.icos-cp.eu/data-products/YVR0-4898) (Drought, 2018 Team & ICOS Ecosystem Thematic Centre, 2020). FluxSat GPP (v1) product was obtained from https://daac.ornl.gov/ (Joiner et al., 2018). GOSIF GPP fluxes were obtained from https://globalecology.unh.edu/data/GOSIF-GPP.html (Li & Xiao, 2019b). CRUNCEP v9 meteorology reanalysis data (Wei et al., 2014) and TRENDY v6 fluxes (Sitch et al., 2015) can be obtained from https://doi.org/10.5281/zenodo.7704810. SPEIbase v2.5 was obtained from https://doi.org/10.20350/digitalCSIC/8508 (Beguería & Vicente-Serrano, 2017). GLEAM v3.3a root-zone soil moisture data were obtained from https://www.gleam.eu/ (Martens et al., 2017). GRACE-REC total terrestrial water storage data were obtained from https://doi.org/10.6084/m9.figshare.7670849 (Humphrey et al., 2017). MOD13C2 v6 data were downloaded from https://ladsweb.modaps.eosdis.nasa.gov/archive/allData/6/MOD13C2/ (Huete et al., 2002). CSIFv2 data were obtained from https://osf.io/8xqy6 (Y. Zhang, 2022). All Python scripts used for the analyses can be obtained from https://github.com/joywei2022/European_Droughts_JAMES (He, 2023).

Acknowledgments
This research is funded by the National Key R&D Program of China (Grant 2020YFA0607504). W. He is funded by the National Natural Science Foundation of China (Grants 41907378 and 42277453) and the Open Funding Project of the State Key Laboratory of Remote Sensing Science (Grant OFSLRSS202012). M. Wu is funded by the National Natural Science Foundation of China (Grant 42111530184). J. Wang is funded by the National Natural Science Foundation of China (Grant 41807434). Y. Zhou is funded by the National Natural Science Foundation of China (Grant 42077419). B. Byrne's research was carried out at the Jet Propulsion Laboratory, California Institute of Technology, under a contract with the National Aeronautics and Space Administration. We gratefully acknowledge the CarbonTracker team of NOAA ESRL, Boulder, Colorado, USA (http://carbontracker.noaa.gov), the CarbonTracker Europe team from Wageningen University, the Netherlands (https://carbontracker.eu), and the CAMS greenhouse gas team for their flux products. We sincerely acknowledge ICOS for sharing the EUROCOM data and Drought-2018 ecosystem eddy covariance flux data. We sincerely acknowledge the TRENDY team and the FLUXCOM team for providing their flux data. We sincerely acknowledge Joanna Joiner from NASA/GSFC for providing the FluxSat GPP product. We acknowledge the Institute Pierre Simon Laplace (IPSL) of France for providing the CRUNCEP reanalysis data. We acknowledge the GLEAM project (https://www.gleam.eu/) for providing satellite soil moisture data. We acknowledge Vincent Humphrey from ETH Zurich for providing the GRACE-REC data. We acknowledge NASA/GSFC for providing the MOD13C2 v6 data. We also acknowledge Yao Zhang from Peking University for providing the CSIF v2 data.

References

Ahlström, A., Raupach, M. R., Schurgers, G., Smith, B., Arneth, A., Jung, M., et al. (2015). The dominant role of semi-arid ecosystems in the trend and variability of the land CO_2 sink. *Science*, *348*(6237), 895–899. https://doi.org/10.1126/science.aaa1668

Alden, C. B., Miller, J. B., Gatti, L. V., Gloor, M. M., Guan, K., Michalak, A. M., et al. (2016). Regional atmospheric CO_2 inversion reveals seasonal and geographic differences in Amazon net biome exchange. *Global Change Biology*, *22*(10), 3427–3443. https://doi.org/10.1111/gcb.13305

Badgley, G., Anderegg, L. D. L., Berry, J. A., & Field, C. B. (2019). Terrestrial gross primary production: Using NIR_V to scale from site to globe. *Global Change Biology*, *25*(11), 3731–3740. https://doi.org/10.1111/gcb.14729

Badgley, G., Field, C. B., & Berry, J. A. (2017). Canopy near-infrared reflectance and terrestrial photosynthesis. *Science Advances*, *3*(3), e1602244. https://doi.org/10.1126/sciadv.1602244

Baldocchi, D. (2008). TURNER REVIEW No. 15. 'Breathing' of the terrestrial biosphere: Lessons learned from a global network of carbon dioxide flux measurement systems. *Australian Journal of Botany*, *56*(1), 1–26. https://doi.org/10.1071/bt07151

Baldocchi, D., Chu, H., & Reichstein, M. (2018). Inter-annual variability of net and gross ecosystem carbon fluxes: A review. *Agricultural and Forest Meteorology*, *249*, 520–533. https://doi.org/10.1016/j.agrformet.2017.05.015

Bastos, A., Fu, Z., Ciais, P., Friedlingstein, P., Sitch, S., Pongratz, J., et al. (2020). Impacts of extreme summers on European ecosystems: A comparative analysis of 2003, 2010 and 2018. *Philosophical Transactions of the Royal Society B: Biological Sciences*, *375*(1810), 20190507. https://doi.org/10.1098/rstb.2019.0507

Beguería, S., & Vicente-Serrano, S. M. (2017). SPEIbase v.2.5 [Dataset]. Digital CSIC. https://doi.org/10.20350/digitalCSIC/8508

Buck. (1996). Buck research CR-1A user's manual. Appendix 1.

Butterfield, Z., Buermann, W., & Keppel-Aleks, G. (2020). Satellite observations reveal seasonal redistribution of northern ecosystem productivity in response to interannual climate variability. *Remote Sensing of Environment*, *242*, 111755. https://doi.org/10.1016/j.rse.2020.111755

Byrne, B., Baker, D. F., Basu, S., Bertolacci, M., Bowman, K. W., Carroll, D., et al. (2023). National CO_2 budgets (2015–2020) inferred from atmospheric CO_2 observations in support of the global stocktake. *Earth System Science Data*, *15*(2), 963–1004. https://doi.org/10.5194/essd-15-963-2023

Byrne, B., Jones, D. B. A., Strong, K., Polavarapu, S. M., Harper, A. B., Baker, D. F., & Maksyutov, S. (2019). On what scales can GOSAT flux inversions constrain anomalies in terrestrial ecosystems? *Atmospheric Chemistry and Physics*, *19*(20), 13017–13035. https://doi.org/10.5194/acp-19-13017-2019

Byrne, B., Liu, J., Bloom, A. A., Bowman, K. W., Butterfield, Z., Joiner, J., et al. (2020). Contrasting regional carbon cycle responses to seasonal climate anomalies across the east-west divide of temperate North America. *Global Biogeochemical Cycles*, *34*(11), e2020GB006598. https://doi.org/10.1029/2020GB006598

Byrne, B., Liu, J., Lee, M., Baker, I., Bowman, K. W., Deutscher, N. M., et al. (2020). Improved constraints on northern extratropical CO_2 fluxes obtained by combining surface-based and space-based atmospheric CO_2 measurements. *Journal of Geophysical Research: Atmospheres*, *125*(15), e2019JD032029. https://doi.org/10.1029/2019JD032029

Chevallier, F., Ciais, P., Conway, T. J., Aalto, T., Anderson, B. E., Bousquet, P., et al. (2010). CO_2 surface fluxes at grid point scale estimated from a global 21 year reanalysis of atmospheric measurements. *Journal of Geophysical Research*, *115*(D21), D21307. https://doi.org/10.1029/2010JD013887

Chevallier, F., Remaud, M., O'Dell, C. W., Baker, D., Peylin, P., & Cozic, A. (2019). Objective evaluation of surface- and satellite-driven carbon dioxide atmospheric inversions. *Atmospheric Chemistry and Physics*, *19*(22), 14233–14251. https://doi.org/10.5194/acp-19-14233-2019

Ciais, P., Reichstein, M., Viovy, N., Granier, A., Ogée, J., Allard, V., et al. (2005). Europe-wide reduction in primary productivity caused by the heat and drought in 2003. *Nature*, *437*(7058), 529–533. https://doi.org/10.1038/nature03972

Dorigo, W., Wagner, W., Albergel, C., Albrecht, F., Balsamo, G., Brocca, L., et al. (2017). ESA CCI soil moisture for improved Earth system understanding: State-of-the art and future directions. *Remote Sensing of Environment*, *203*, 185–215. https://doi.org/10.1016/j.rse.2017.07.001

Drought 2018 TeamICOS Ecosystem Thematic Centre. (2020). Drought-2018 ecosystem eddy covariance flux product for 52 stations in FLUXNET-Archive format [Dataset]. ICOS Carbon Portal. https://doi.org/10.18160/YVR0-4898

Flach, M., Sippel, S., Gans, F., Bastos, A., Brenning, A., Reichstein, M., & Mahecha, M. D. (2018). Contrasting biosphere responses to hydrometeorological extremes: Revisiting the 2010 western Russian heatwave. *Biogeosciences*, *15*(20), 6067–6085. https://doi.org/10.5194/bg-15-6067-2018

Fortems-Cheiney, A., Pison, I., Broquet, G., Dufour, G., Berchet, A., Potier, E., et al. (2021). Variational regional inverse modeling of reactive species emissions with PYVAR-CHIMERE-v2019. *Geoscientific Model Development*, *14*(5), 2939–2957. https://doi.org/10.5194/gmd-14-2939-2021

Friedlingstein, P., Jones, M. W., O'Sullivan, M., Andrew, R. M., Hauck, J., Peters, G. P., et al. (2019). Global carbon budget 2019. *Earth System Science Data*, *11*(4), 1783–1838. https://doi.org/10.5194/essd-11-1783-2019

Guanter, L., Zhang, Y., Jung, M., Joiner, J., Voigt, M., Berry, J. A., et al. (2014). Global and time-resolved monitoring of crop photosynthesis with chlorophyll fluorescence. *Proceedings of the National Academy of Sciences of the United States of America*, *111*(14), 1327–1333. https://doi.org/10.1073/pnas.1320008111

Gurney, K. R., Law, R. M., Denning, A. S., Rayner, P. J., Pak, B. C., Baker, D., et al. (2004). Transcom 3 inversion intercomparison: Model mean results for the estimation of seasonal carbon sources and sinks. *Global Biogeochemical Cycles*, *18*(1), GB1010. https://doi.org/10.1029/2003GB002111

Hansen, J., Ruedy, R., Sato, M., & Lo, K. (2010). Global surface temperature change. *Reviews of Geophysics*, *48*(4), RG4004. https://doi.org/10.1029/2010RG000345

He, W. (2023). joywei2022/European_Droughts_JAMES: Version 1.0.0 [Software]. GitHub. Retrieved from https://github.com/joywei2022/European_Droughts_JAMES

He, W., Jiang, F., & Ju, W. (2022). Global net ecosystem exchange of CO_2 inferred from the OCO-2 XCO_2 retrievals (GCAS OCO-2 inversion) [Dataset]. Zenodo. https://doi.org/10.5281/zenodo.7040223

He, W., Jiang, F., Wu, M., Ju, W., Scholze, M., Chen, J. M., et al. (2022). China's terrestrial carbon sink over 2010–2015 constrained by satellite observations of atmospheric CO_2 and land surface variables. *Journal of Geophysical Research: Biogeosciences*, *127*(2), e2021JG006644. https://doi.org/10.1029/2021JG006644

He, W., Ju, W., Jiang, F., Parazoo, N., Gentine, P., Wu, X., et al. (2021). Peak growing season patterns and climate extremes-driven responses of gross primary production estimated by satellite and process based models over North America. *Agricultural and Forest Meteorology*, *298–299*, 108292. https://doi.org/10.1016/j.agrformet.2020.108292

He, W., Ju, W., Schwalm, C. R., Sippel, S., Wu, X., He, Q., et al. (2018). Large-scale droughts responsible for dramatic reductions of terrestrial net carbon uptake over North America in 2011 and 2012. *Journal of Geophysical Research: Biogeosciences*, *123*(7), 2053–2071. https://doi.org/10.1029/2018jg004520

He, W., van der Velde, I. R., Andrews, A. E., Sweeney, C., Miller, J., Tans, P., et al. (2018). CTDAS-Lagrange v1.0: A high-resolution data assimilation system for regional carbon dioxide observations. *Geoscientific Model Development*, *11*(8), 3515–3536. https://doi.org/10.5194/gmd-11-3515-2018

Heimann, M., & Korner, S. (2003). *The global atmospheric tracer model TM3Rep* (Vol. 5, pp. 1–131). Max-Planck-Institut für Biogeochemie.

Heiskanen, J., Brümmer, C., Buchmann, N., Calfapietra, C., Chen, H., Gielen, B., et al. (2021). The integrated carbon observation system in Europe. *Bulletin of the American Meteorological Society*, *103*(3), 1–54. https://doi.org/10.1175/bams-d-19-0364.1

Huete, A., Didan, K., Miura, T., Rodriguez, E. P., Gao, X., & Ferreira, L. G. (2002). Overview of the radiometric and biophysical performance of the MODIS vegetation indices. *Remote Sensing of Environment*, *83*(1), 195–213. https://doi.org/10.1016/s0034-4257(02)00096-2

Humphrey, V., Gudmundsson, L., & Seneviratne, S. I. (2017). A global reconstruction of ICOS-Drought2018 (2020), Drought-2018 ecosystem eddy covariance flux product for 52 stations in FLUXNET-Archive format [Dataset]. Drought 2018 Team and ICOS Ecosystem Thematic Centre. https://doi.org/10.18160/YVR0-4898

Ishizawa, M., Mabuchi, K., Shirai, T., Inoue, M., Morino, I., Uchino, O., et al. (2016). Inter-annual variability of summertime CO_2 exchange in Northern Eurasia inferred from GOSAT XCO_2. *Environmental Research Letters*, *11*(10), 105001. https://doi.org/10.1088/1748-9326/11/10/105001

Jacobson, A. R., Schuldt, K. N., Miller, J. B., Oda, T., Tans, P., Andrews, A., et al. (2020). *Carbontracker CT2019, model published 2020*. NOAA Earth System Research Laboratory, Global Monitoring Division. https://doi.org/10.25925/39m3-6069

Jain, A. K., Meiyappan, P., Song, Y., & House, J. I. (2013). CO_2 emissions from land-use change affected more by nitrogen cycle, than by the choice of land-cover data. *Global Change Biology*, *19*(9), 2893–2906. https://doi.org/10.1111/gcb.12207

Jiang, F. (2021). Regional CO_2 fluxes from 2010 to 2015 inferred from GOSAT XCO_2 retrievals using a new version of the Global Carbon Assimilation System [Dataset]. Zenodo. https://doi.org/10.5281/zenodo.5829774

Jiang, F., He, W., Ju, W., Wang, H., Wu, M., Wang, J., et al. (2022). The status of carbon neutrality of the world's top 5 CO_2 emitters as seen by carbon satellites. *Fundamental Research*, *2*(3), 357–366. https://doi.org/10.1016/j.fmre.2022.02.001

Jiang, F., Ju, W., He, W., Wu, M., Wang, H., Wang, J., et al. (2022). A ten-year global monthly averaged terrestrial NEE inferred from the ACOS GOSAT v9 XCO_2 retrievals (GCAS2021). *Earth System Science Data Discussions*, *2022*, 1–38. https://doi.org/10.5194/essd-2022-15

Jiang, F., Wang, H., Chen, J. M., Ju, W., Tian, X., Feng, S., et al. (2021). Regional CO_2 fluxes from 2010 to 2015 inferred from GOSAT XCO_2 retrievals using a new version of the Global Carbon Assimilation System. *Atmospheric Chemistry and Physics*, *21*(3), 1963–1985. https://doi.org/10.5194/acp-21-1963-2021

Joiner, J., Yoshida, Y., Zhang, Y., Duveiller, G., Jung, M., Lyapustin, A., et al. (2018). Estimation of terrestrial global gross primary production (GPP) with satellite data-driven models and eddy covariance flux data. *Remote Sensing*, *10*(9), 1346. https://doi.org/10.3390/rs10091346

Jung, M., Koirala, S., Weber, U., Ichii, K., Gans, F., Camps-Valls, G., et al. (2019). The FLUXCOM ensemble of global land-atmosphere energy fluxes. *Scientific Data*, *6*(1), 74. https://doi.org/10.1038/s41597-019-0076-8

Jung, M., Schwalm, C., Migliavacca, M., Walther, S., Camps-Valls, G., Koirala, S., et al. (2020). Scaling carbon fluxes from eddy covariance sites to globe: Synthesis and evaluation of the FLUXCOM approach. *Biogeosciences*, *17*(5), 1343–1365. https://doi.org/10.5194/bg-17-1343-2020

Kato, E., Kinoshita, T., Ito, A., Kawamiya, M., & Yamagata, Y. (2013). Evaluation of spatially explicit emission scenario of land-use change and biomass burning using a process-based biogeochemical model. *Journal of Land Use Science*, *8*(1), 104–122. https://doi.org/10.1080/1747423x.2011.628705

Kiel, M., Eldering, A., Roten, D. D., Lin, J. C., Feng, S., Lei, R., et al. (2021). Urban-focused satellite CO_2 observations from the orbiting carbon Observatory-3: A first look at the Los Angeles megacity. *Remote Sensing of Environment*, *258*, 112314. https://doi.org/10.1016/j.rse.2021.112314

Knorr, W. (2000). Annual and interannual CO_2 exchanges of the terrestrial biosphere: Process-based simulations and uncertainties. *Global Ecology and Biogeography*, *9*(3), 225–252. https://doi.org/10.1046/j.1365-2699.2000.00159.x

Kountouris, P., Gerbig, C., Rödenbeck, C., Karstens, U., Koch, T. F., & Heimann, M. (2018). Atmospheric CO_2 inversions on the mesoscale using data-driven prior uncertainties: Quantification of the European terrestrial CO_2 fluxes. *Atmospheric Chemistry and Physics*, *18*(4), 3047–3064. https://doi.org/10.5194/acp-18-3047-2018

Krinner, G., Viovy, N., de Noblet-Ducoudré, N., Ogée, J., Polcher, J., Friedlingstein, P., et al. (2005). A dynamic global vegetation model for studies of the coupled atmosphere-biosphere system. *Global Biogeochemical Cycles*, *19*(1), GB1015. https://doi.org/10.1029/2003GB002199

Kuhlmann, G., Brunner, D., Broquet, G., & Meijer, Y. (2020). Quantifying CO_2 emissions of a city with the Copernicus Anthropogenic CO_2 Monitoring satellite mission. *Atmospheric Measurement Techniques*, *13*(12), 6733–6754. https://doi.org/10.5194/amt-13-6733-2020

Kwon, M. J., Ballantyne, A., Ciais, P., Bastos, A., Chevallier, F., Liu, Z., et al. (2021). Siberian 2020 heatwave increased spring CO_2 uptake but not annual CO_2 uptake. *Environmental Research Letters*, *16*(12), 124030. https://doi.org/10.1088/1748-9326/ac358b

Laaha, G., Gauster, T., Tallaksen, L. M., Vidal, J. P., Stahl, K., Prudhomme, C., et al. (2017). The European 2015 drought from a hydrological perspective. *Hydrology and Earth System Sciences*, *21*(6), 3001–3024. https://doi.org/10.5194/hess-21-3001-2017

Lasslop, G., Reichstein, M., Papale, D., Richardson, A. D., Arneth, A., Barr, A., et al. (2010). Separation of net ecosystem exchange into assimilation and respiration using a light response curve approach: Critical issues and global evaluation. *Global Change Biology*, *16*(1), 187–208. https://doi.org/10.1111/j.1365-2486.2009.02041.x

Lee, E., Zeng, F.-W., Koster, R. D., Ott, L. E., Mahanama, S., Weir, B., et al. (2020). Impact of a regional U.S. Drought on land and atmospheric carbon. *Journal of Geophysical Research: Biogeosciences*, *125*(8), e2019JG005599. https://doi.org/10.1029/2019JG005599

Lee, J.-E., Frankenberg, C., van der Tol, C., Berry, J. A., Guanter, L., Boyce, C. K., et al. (2013). Forest productivity and water stress in Amazonia: Observations from GOSAT chlorophyll fluorescence. *Proceedings of the Royal Society of London B Biological Sciences*, *280*(1761), 20130171. https://doi.org/10.1098/rspb.2013.0171

Lenssen, N. J. L., Schmidt, G. A., Hansen, J. E., Menne, M. J., Persin, A., Ruedy, R., & Zyss, D. (2019). Improvements in the GISTEMP uncertainty model. *Journal of Geophysical Research: Atmospheres*, *124*(12), 6307–6326. https://doi.org/10.1029/2018JD029522

Li, X., & Xiao, J. (2019a). A global, 0.05-degree product of solar-induced chlorophyll fluorescence derived from OCO-2, MODIS, and reanalysis data. *Remote Sensing*, *11*(5), 517. https://doi.org/10.3390/rs11050517

Li, X., & Xiao, J. (2019b). Mapping photosynthesis solely from solar-induced chlorophyll fluorescence: A global, fine-resolution dataset of gross primary production derived from OCO-2. *Remote Sensing*, *11*(21), 2563. https://doi.org/10.3390/rs11212563

Li, X., Xiao, J., He, B., Altaf Arain, M., Beringer, J., Desai, A. R., et al. (2018). Solar-induced chlorophyll fluorescence is strongly correlated with terrestrial photosynthesis for a wide variety of biomes: First global analysis based on OCO-2 and flux tower observations. *Global Change Biology*, *24*(9), 3990–4008. https://doi.org/10.1111/gcb.14297

Liu, J., Baskaran, L., Bowman, K., Schimel, D., Bloom, A. A., Parazoo, N. C., et al. (2020). Carbon monitoring system flux net biosphere exchange 2020 (CMS-Flux NBE 2020). *Earth System Science Data*, *13*(2), 299–330. https://doi.org/10.5194/essd-13-299-2021

Liu, J., Bowman, K., Parazoo, N. C., Bloom, A. A., Wunch, D., Jiang, Z., et al. (2018). Detecting drought impact on terrestrial biosphere carbon fluxes over contiguous US with satellite observations. *Environmental Research Letters*, *13*(9), 095003. https://doi.org/10.1088/1748-9326/aad5ef

Liu, J., Bowman, K. W., Schimel, D. S., Parazoo, N. C., Jiang, Z., Lee, M., et al. (2017). Contrasting carbon cycle responses of the tropical continents to the 2015–2016 El Niño. *Science*, *358*(6360), eaam5690. https://doi.org/10.1126/science.aam5690

Liu, Y., Wang, J., Yao, L., Chen, X., Cai, Z., Yang, D., et al. (2018). The TanSat mission: Preliminary global observations. *Science Bulletin*, *63*(18), 1200–1207. https://doi.org/10.1016/j.scib.2018.08.004

Martens, B., Gonzalez Miralles, D., Lievens, H., van der Schalie, R., de Jeu, R. A., Fernández-Prieto, D., et al. (2017). GLEAM v3: Satellite-based land evaporation and root-zone soil moisture. *Geoscientific Model Development*, *10*(5), 1903–1925. https://doi.org/10.5194/gmd-10-1903-2017

Meesters, A. G. C. A., Tolk, L. F., Peters, W., Hutjes, R. W. A., Vellinga, O. S., Elbers, J. A., et al. (2012). Inverse carbon dioxide flux estimates for The Netherlands. *Journal of Geophysical Research*, *117*(D20), D20306. https://doi.org/10.1029/2012JD017797

Miralles, D. G., Holmes, T. R. H., De Jeu, R. A. M., Gash, J. H., Meesters, A. G. C. A., & Dolman, A. J. (2011). Global land-surface evaporation estimated from satellite-based observations. *Hydrology and Earth System Sciences*, *15*(2), 453–469. https://doi.org/10.5194/hess-15-453-2011

Molina, L., Broquet, G., Imbach, P., Chevallier, F., Poulter, B., Bonal, D., et al. (2015). On the ability of a global atmospheric inversion to constrain variations of CO_2 fluxes over Amazonia. *Atmospheric Chemistry and Physics*, *15*(14), 8423–8438. https://doi.org/10.5194/acp-15-8423-2015

Monteil, G., Broquet, G., Scholze, M., Lang, M., Gerbig, C., Koch, F.-T., et al. (2019). EUROCOM ensemble of inversion results for 2006–2015 [Dataset]. ICOS Carbon Portal. https://doi.org/10.18160/E72F-D093

Monteil, G., Broquet, G., Scholze, M., Lang, M., Karstens, U., Gerbig, C., et al. (2020). The regional European atmospheric transport inversion comparison, EUROCOM: First results on European-wide terrestrial carbon fluxes for the period 2006–2015. *Atmospheric Chemistry and Physics*, *20*(20), 12063–12091. https://doi.org/10.5194/acp-20-12063-2020

Monteil, G., & Scholze, M. (2021). Regional CO_2 inversions with LUMIA, the Lund University modular inversion algorithm, v1.0. *Geoscientific Model Development*, *14*(6), 3383–3406. https://doi.org/10.5194/gmd-2019-227

Monteith, J. L., & Unsworth, M. H. (2008). *Principles of environmental physics* (3rd ed., p. 418). Academic Press.

Moore, B., Crowell, S., Rayner, P., Kumer, J., O'Dell, C., O'Brien, D., et al. (2018). The potential of the geostationary carbon cycle observatory (GeoCarb) to provide multi-scale constraints on the carbon cycle in the Americas. *Frontiers in Environmental Science*, *6*, 109. https://doi.org/10.3389/fenvs.2018.00109

New, M., Hulme, M., & Jones, P. (2000). Representing twentieth-century space–time climate variability. Part II: Development of 1901–96 monthly grids of terrestrial surface climate. *Journal of Climate*, *13*(13), 2217–2238. https://doi.org/10.1175/1520-0442(2000)013<2217:rtcstc>2.0.co;2

Palmer, P. I. (2018). The role of satellite observations in understanding the impact of El Niño on the carbon cycle: Current capabilities and future opportunities. *Philosophical Transactions of the Royal Society B: Biological Sciences*, *373*(1760), 20170407. https://doi.org/10.1098/rstb.2017.0407

Peters, W., Bastos, A., Ciais, P., & Vermeulen, A. (2020). A historical, geographical and ecological perspective on the 2018 European summer drought. *Philosophical Transactions of the Royal Society B: Biological Sciences*, *375*(1810), 20190505. https://doi.org/10.1098/rstb.2019.0505

Peters, W., Jacobson, A. R., Sweeney, C., Andrews, A. E., Conway, T. J., Masarie, K., et al. (2007). An atmospheric perspective on North American carbon dioxide exchange: CarbonTracker. *Proceedings of the National Academy of Sciences of the United States of America*, *104*(48), 18925–18930. https://doi.org/10.1073/pnas.0708986104

Peters, W., Krol, M., Van Der Werf, G., Houweling, S., Jones, C., Hughes, J., et al. (2010). Seven years of recent European net terrestrial carbon dioxide exchange constrained by atmospheric observations. *Global Change Biology*, *16*(4), 1317–1337. https://doi.org/10.1111/j.1365-2486.2009.02078.x

Peters, W., Miller, J. B., Whitaker, J., Denning, A. S., Hirsch, A., Krol, M. C., et al. (2005). An ensemble data assimilation system to estimate CO_2 surface fluxes from atmospheric trace gas observations. *Journal of Geophysical Research*, *110*(D24), D24304. https://doi.org/10.1029/2005JD006157

Peters, W., van der Velde, I. R., van Schaik, E., Miller, J. B., Ciais, P., Duarte, H. F., et al. (2018). Increased water-use efficiency and reduced CO_2 uptake by plants during droughts at a continental scale. *Nature Geoscience*, *11*(10), 744–748. https://doi.org/10.1038/s41561-018-0212-7

Peylin, P., Law, R., Gurney, K., Chevallier, F., Jacobson, A., Maki, T., et al. (2013). Global atmospheric carbon budget: Results from an ensemble of atmospheric CO_2 inversions. *Biogeosciences*, *10*, 6699–6720. https://doi.org/10.5194/bg-10-6699-2013

Piao, S., Wang, X., Wang, K., Li, X., Bastos, A., Canadell, J. G., et al. (2020). Interannual variation of terrestrial carbon cycle: Issues and perspectives. *Global Change Biology*, *26*(1), 300–318. https://doi.org/10.1111/gcb.14884

Rayner, P., Scholze, M., Knorr, W., Kaminski, T., Giering, R., & Widmann, H. (2005). Two decades of terrestrial carbon fluxes from a carbon cycle data assimilation system (CCDAS). *Global Biogeochemical Cycles*, *19*(2), GB2026. https://doi.org/10.1029/2004GB002254

Reichstein, M., Falge, E., Baldocchi, D., Papale, D., Aubinet, M., Berbigier, P., et al. (2005). On the separation of net ecosystem exchange into assimilation and ecosystem respiration: Review and improved algorithm. *Global Change Biology*, *11*(9), 1424–1439. https://doi.org/10.1111/j.1365-2486.2005.001002.x

Rödenbeck, C., Houweling, S., Gloor, M., & Heimann, M. (2003). CO_2 flux history 1982–2001 inferred from atmospheric data using a global inversion of atmospheric transport. *Atmospheric Chemistry and Physics*, *3*(6), 1919–1964. https://doi.org/10.5194/acp-3-1919-2003

Rödenbeck, C., Zaehle, S., Keeling, R., & Heimann, M. (2018a). History of El Niño impacts on the global carbon cycle 1957–2017: A quantification from atmospheric CO_2 data. *Philosophical Transactions of the Royal Society B: Biological Sciences*, *373*(1760), 20170303. https://doi.org/10.1098/rstb.2017.0303

Rödenbeck, C., Zaehle, S., Keeling, R., & Heimann, M. (2018b). How does the terrestrial carbon exchange respond to inter-annual climatic variations? A quantification based on atmospheric CO_2 data. *Biogeosciences*, *15*(8), 2481–2498. https://doi.org/10.5194/bg-15-2481-2018

Rödenbeck, C., Zaehle, S., Keeling, R., & Heimann, M. (2020). The European carbon cycle response to heat and drought as seen from atmospheric CO_2 data for 1999–2018. *Philosophical Transactions of the Royal Society B: Biological Sciences*, *375*(1810), 20190506. https://doi.org/10.1098/rstb.2019.0506

Schewe, J., Gosling, S. N., Reyer, C., Zhao, F., Ciais, P., Elliott, J., et al. (2019). State-of-the-art global models underestimate impacts from climate extremes. *Nature Communications*, *10*(1), 1005. https://doi.org/10.1038/s41467-019-08745-6

Scholze, M., Kaminski, T., Knorr, W., Voßbeck, M., Wu, M., Ferrazzoli, P., et al. (2019). Mean European carbon sink over 2010–2015 estimated by simultaneous assimilation of atmospheric CO_2, soil moisture, and vegetation optical depth. *Geophysical Research Letters*, *46*(23), 13796–13803. https://doi.org/10.1029/2019GL085725

Shiga, Y. P., Tadić, J. M., Qiu, X., Yadav, V., Andrews, A. E., Berry, J. A., & Michalak, A. M. (2018). Atmospheric CO_2 observations reveal strong correlation between regional net biospheric carbon uptake and solar-induced chlorophyll fluorescence. *Geophysical Research Letters*, *45*(2), 1122–1132. https://doi.org/10.1002/2017GL076630

Sitch, S., Friedlingstein, P., Gruber, N., Jones, S., Murray-Tortarolo, G., Ahlström, A., et al. (2015). Recent trends and drivers of regional sources and sinks of carbon dioxide. *Biogeosciences*, *12*(3), 653–679. https://doi.org/10.5194/bg-12-653-2015

Smith, N. E., Kooijmans, L. M. J., Koren, G., Schaik, E. V., Woude, A. V. M. D., Wanders, N., et al. (2020). Spring enhancement and summer reduction in carbon uptake during the 2018 drought in northwestern Europe. *Philosophical Transactions of the Royal Society B: Biological Sciences*, *375*(1810), 20190509. https://doi.org/10.1098/rstb.2019.0509

Song, L., Guanter, L., Guan, K., You, L., Huete, A., Ju, W., & Zhang, Y. (2018). Satellite sun-induced chlorophyll fluorescence detects early response of winter wheat to heat stress in the Indian Indo-Gangetic Plains. *Global Change Biology*, *24*(9), 4023–4037. https://doi.org/10.1111/gcb.14302

Souza, A. G. S. S., Neto, A. R., Rossato, L., Alvalá, R. C. S., & Souza, L. L. (2018). Use of SMOS L3 soil moisture data: Validation and drought assessment for Pernambuco State, Northeast Brazil. *Remote Sensing*, *10*(8), 1314. https://doi.org/10.3390/rs10081314

Sun, Y., Fu, R., Dickinson, R., Joiner, J., Frankenberg, C., Gu, L., et al. (2015). Drought onset mechanisms revealed by satellite solar-induced chlorophyll fluorescence: Insights from two contrasting extreme events. *Journal of Geophysical Research: Biogeosciences*, *120*(11), 2427–2440. https://doi.org/10.1002/2015jg003150

Suto, H., Kataoka, F., Kikuchi, N., Knuteson, R. O., Butz, A., Haun, M., et al. (2021). Thermal and near-infrared sensor for carbon observation Fourier transform spectrometer-2 (TANSO-FTS-2) on the Greenhouse gases Observing SATellite-2 (GOSAT-2) during its first year in orbit. *Atmospheric Measurement Techniques*, *14*(3), 2013–2039. https://doi.org/10.5194/amt-14-2013-2021

Teuling, A. J., Seneviratne, S. I., Stöckli, R., Reichstein, M., Moors, E., Ciais, P., et al. (2010). Contrasting response of European forest and grassland energy exchange to heatwaves. *Nature Geoscience*, *3*(10), 722–727. https://doi.org/10.1038/ngeo950

Thompson, R. L., Broquet, G., Gerbig, C., Koch, T., Lang, M., Monteil, G., et al. (2020). Changes in net ecosystem exchange over Europe during the 2018 drought based on atmospheric observations. *Philosophical Transactions of the Royal Society B: Biological Sciences*, *375*(1810), 20190512. https://doi.org/10.1098/rstb.2019.0512

Thompson, R. L., & Stohl, A. (2014). FLEXINVERT: An atmospheric Bayesian inversion framework for determining surface fluxes of trace species using an optimized grid. *Geoscientific Model Development*, *7*(5), 2223–2242. https://doi.org/10.5194/gmd-7-2223-2014

Tian, H., Chen, G., Lu, C., Xu, X., Hayes, D. J., Ren, W., et al. (2015). North American terrestrial CO_2 uptake largely offset by CH_4 and N_2O emissions: Toward a full accounting of the greenhouse gas budget. *Climatic Change*, *129*(3–4), 413–426. https://doi.org/10.1007/s10584-014-1072-9

Tramontana, G., Jung, M., Schwalm, C. R., Ichii, K., Camps-Valls, G., Ráduly, B., et al. (2016). Predicting carbon dioxide and energy fluxes across global FLUXNET sites with regression algorithms. *Biogeosciences*, *13*(14), 4291–4313. https://doi.org/10.5194/bg-13-4291-2016

van der Laan-Luijkx, I. T., van der Velde, I. R., Krol, M. C., Gatti, L. V., Domingues, L. G., Correia, C. S. C., et al. (2015). Response of the Amazon carbon balance to the 2010 drought derived with CarbonTracker South America. *Global Biogeochemical Cycles*, *29*(7), 1092–1108. https://doi.org/10.1002/2014gb005082

van der Laan-Luijkx, I. T., van der Velde, I. R., van der Veen, E., Tsuruta, A., Stanislawska, K., Babenhauserheide, A., et al. (2017). The CarbonTracker data assimilation shell (CTDAS) v1.0: Implementation and global carbon balance 2001–2015. *Geoscientific Model Development*, *10*(7), 2785–2800. https://doi.org/10.5194/gmd-10-2785-2017

Wang, S., Zhang, Y., Ju, W., Porcar-Castell, A., Ye, S., Zhang, Z., et al. (2020). Warmer spring alleviated the impacts of 2018 European summer heatwave and drought on vegetation photosynthesis. *Agricultural and Forest Meteorology*, *295*, 108195. https://doi.org/10.1016/j.agrformet.2020.108195

Wang, Y., Law, R., & Pak, B. (2010). A global model of carbon, nitrogen and phosphorus cycles for the terrestrial biosphere. *Biogeosciences*, *7*(7), 2261–2282. https://doi.org/10.5194/bg-7-2261-2010

Wei, Y., Liu, S., Huntzinger, D. N., Michalak, A. M., Viovy, N., Post, W. M., et al. (2014). The North American carbon Program multi-scale synthesis and terrestrial model intercomparison project - Part 2: Environmental driver data. *Geoscientific Model Development*, *6*(4), 5375–5422. https://doi.org/10.5194/gmd-7-2875-2014

Wieder, W. R., Butterfield, Z., Lindsay, K., Lombardozzi, D. L., & Keppel-Aleks, G. (2021). Interannual and seasonal drivers of carbon cycle variability represented by the Community Earth System Model (CESM2). *Global Biogeochemical Cycles*, *35*(9), e2021GB007034. https://doi.org/10.1029/2021GB007034

Wigneron, J.-P., Li, X., Frappart, F., Fan, L., Al-Yaari, A., De Lannoy, G., et al. (2021). SMOS-IC data record of soil moisture and L-VOD: Historical development, applications and perspectives. *Remote Sensing of Environment*, *254*, 112238. https://doi.org/10.1016/j.rse.2020.112238

Wolf, S., Keenan, T. F., Fisher, J. B., Baldocchi, D. D., Desai, A. R., Richardson, A. D., et al. (2016). Warm spring reduced carbon cycle impact of the 2012 US summer drought. *Proceedings of the National Academy of Sciences of the United States of America*, *113*(21), 5880–5885. https://doi.org/10.1073/pnas.1519620113

Wu, M., Scholze, M., Kaminski, T., Voßbeck, M., & Tagesson, T. (2020). Using SMOS soil moisture data combining CO_2 flask samples to constrain carbon fluxes during 2010–2015 within a Carbon Cycle Data Assimilation System (CCDAS). *Remote Sensing of Environment*, *240*, 111719. https://doi.org/10.1016/j.rse.2020.111719

Xiao, J., Liu, S., & Stoy, P. C. (2016). Preface: Impacts of extreme climate events and disturbances on carbon dynamics. *Biogeosciences*, *13*(12), 3665–3675. https://doi.org/10.5194/bg-13-3665-2016

Yin, Y., Byrne, B., Liu, J., Wennberg, P., Davis, K. J., Magney, T., et al. (2020). Cropland carbon uptake delayed and reduced by 2019 Midwest floods. *AGU Advances*, *1*(1), e2019AV000140. https://doi.org/10.1029/2019AV000140

Zahradníček, P., Trnka, M., Brázdil, R., Možný, M., Štěpánek, P., Hlavinka, P., et al. (2015). The extreme drought episode of August 2011–May 2012 in the Czech Republic. *International Journal of Climatology*, *35*(11), 3335–3352. https://doi.org/10.1002/joc.4211

Zeng, N., Mariotti, A., & Wetzel, P. (2005). Terrestrial mechanisms of interannual CO_2 variability. *Global Biogeochemical Cycles*, *19*(1), GB1016. https://doi.org/10.1029/2004GB002273

Zeng, Y., Badgley, G., Dechant, B., Ryu, Y., Chen, M., & Berry, J. A. (2019). A practical approach for estimating the escape ratio of near-infrared solar-induced chlorophyll fluorescence. *Remote Sensing of Environment*, *232*, 111209. https://doi.org/10.1016/j.rse.2019.05.028

Zhang, L., Ren, X., Wang, J., He, H., Wang, S., Wang, M., et al. (2019). Interannual variability of terrestrial net ecosystem productivity over China: Regional contributions and climate attribution. *Environmental Research Letters*, *14*(1), 014003. https://doi.org/10.1088/1748-9326/aaec95

Zhang, Y. (2022). Contiguous solar induced chlorophyll fluorescence (CSIF) [Dataset]. OSF. https://doi.org/10.17605/OSF.IO/8XQY6

Zhang, Y., Joiner, J., Alemohammad, S. H., Zhou, S., & Gentine, P. (2018). A global spatially contiguous solar-induced fluorescence (CSIF) dataset using neural networks. *Biogeosciences*, *15*(19), 5779–5800. https://doi.org/10.5194/bg-15-5779-2018